Journal of Medicinal Chemistry

Article

Chlorin p6-based Water-soluble Amino Acid Derivatives as Potent Photosensitizers for Photodynamic Therapy

Zhi Meng, Bin Yu, Guiyan Han, Minghui Liu, Bin Shan, Guoqiang Dong, Zhenyuan Miao, Ningyang Jia, Zou Tan, Buhong Li, Wannian Zhang, Haiying Zhu, Chunquan Sheng, and Jianzhong Yao

J. Med. Chem., **Just Accepted Manuscript** • DOI: 10.1021/acs.jmedchem.6b00352 • Publication Date (Web): 02 May 2016

ACS Publications

Journal of Medicinal Chemistry is published by the American Chemical Society. 1155 Sixteenth Street N.W., Washington, DC 20036

Chlorin p_6-based Water-soluble Amino Acid Derivatives as Potent Photosensitizers for Photodynamic Therapy

Zhi Meng[†,1], Bin Yu[†,2], Guiyan Han[†,1], Minghui Liu[3], Bin Shan[3], Guoqiang Dong[1], Zhenyuan Miao[1], Ningyang Jia[4], Zou Tan[5], Buhong Li[5], Wannian Zhang[1], Haiying Zhu[*,2], Chunquan Sheng[*,1], Jianzhong Yao[*,1]

[1]School of Pharmacy, Second Military Medical University, 325 Guohe Road, Shanghai 200433, China

[2]Department of Cell Biology, Second Military Medical University, 800 Xiangyin Road, Shanghai 200433, China

[3]Department of Pharmacy, Fujian University of Traditional Chinese Medicine, 1 Qiuyang Road, Fuzhou, 350122, China

[4]Department of Radiology, Shanghai Eastern Hepatobiliary Surgery Hospital, Second Military Medical University, 225 Changhai Road, Shanghai 200438, China

[5]Key Laboratory of OptoElectronic Science and Technology for Medicine of Ministry of Education, Fujian Normal University, 32 Shangshan Road, Fujian 350007, China

---

ABSTRACT: The development of novel photosensitizer with high phototoxicity, low dark-toxicity and good water solubility is a challenging task for photodynamic therapy (PDT). A series of chlorin p_6-based water-soluble amino acid conjugates were synthesized and investigated for antitumor activity. Among them, aspartylchlorin p_6 dimethylester (**7b**) showed highest phototoxicity against melanoma cells with weakest dark-toxicity, which was more phototoxic than verteporfin while with less dark-toxicity. It also exhibited better *in vivo* PDT antitumor efficacy on mice bearing B16-F10 tumor than verteporfin. The biological assays revealed that **7b** was localized in multiple subcellular organelles, and could cause both cell necrosis and apoptosis after PDT in a dose dependent

manner, resulting in more effective cell destruction. As a result, **7b** represents a promising photosensitizer for PDT applications because of its strong absorption in the phototherapeutic window, relatively high singlet oxygen quantum yield, highest dark-toxicity/phototoxicity ratio, good water-solubility and excellent *in vivo* PDT antitumor efficacy.

INTRODUCTION

PDT is clinically approved, minimally invasive protocol for the treatment that can be curative of early disease and palliative in advanced disease.[1-4] It is a photochemistry-based treatment procedure in which the photosensitizer (PS) is typically administered intravenously or topically, and after a time named the drug-to-light interval (DLI), PS is activated by light of an appropriate wavelength (*e.g.* phototherapeutic window 650~850 nm) to form an excited triplet state. Excited PS molecular transfers an electron to molecular oxygen or other electron acceptors generating superoxide anions and radicals (type I reaction), or transfers its energy to the triplet ground state of molecular oxygen to produce the highly cytotoxic singlet oxygen (type II reaction) with the ultimate formation of reactive oxygen species (ROS). ROS mainly initiates three biological mechanisms that make PDT an effective anticancer procedure: 1) direct tumor killing induced by the ROS; 2) tumor-associated vascular shutdown and massive ischemice death; 3) activation of antitumor immune memory and systemic response.[5-13]

Photofrin, the first generation of porphyrin-type PS, has achieved some clinical efficacy, but it also suffered from several drawbacks such as chemical heterogeneity, poor tissue penetration due to its limited maximum absorption wavelength, weak absorption at therapeutic wave length (630 nm), and prolonged cutaneous photosensitivity caused by its slow elimination in normal tissue.[14] Compared to porphyrins, chlorin-type PSs are receiving considerable attention owing to their intense absorption in near infrared region ($\geq$ 650 nm, also called "phototherapeutic window"), which are relatively harmless and penetrate deeply in biological tissues. In particular, chlorophyll *a* derivatives are inherently amphiphilic macrocycles that have been extensively investigated. As

compared to commercial photofrin, chlorophyll *a* derivatives generally showed low dark toxicities, rapid clearance from normal tissue and low cutaneous phototoxicity. However, poor water solubility is the main limitation of the chlorophyll *a* derivatives, which has hampered their PDT clinical application. Thus, chlorophyll *a* analogues of the chlorin e_6 series have been derivatized in multiple ways to produce novel water-soluble PSs for PDT investigations. For this, chlorophyll *a* derivatives have been conjugated to amino acids, peptides and sugars have been reported. Among them, talaporfin [15, 16] and verteporfin [17, 18] were approved for PDT treatment. In addition, bacteriochlorin-type PSs received intensive attention mainly due to their advantage of intense absorption in near infrared region (740~780 nm), which penetrate more deeply in biological tissues than chlorins, and Pd-bacteriopheophorbide, padeliporfin and redaporfin have entered clinical trials.[5,6,19-25]

In our previous studies, a series of novel chlorin-type PSs such as benzochloroporphyrin derivatives (BCPDs) were designed and synthesized using crude chlorophyll extracts from Chinese traditional herb named silkworm excrement as the starting material.[26] Among them, benzochloroporphyrin p_6 dimethylester *cis*-isomer (BCPD-18MA, **11**) was a potent antitumor candidate for PDT due to its good photobiological properties, but its water solubility remained to be further improved.[27] Introducing amino acids was reported to be an effective strategy to improve the water solubility and the biological effects of chlorin- and porphyrin-based derivatives.[28-32] Inspired by these encouraging results, herein we synthesized a series of new water-soluble amino acid conjugates of **11** and chlorin p_6 dimethylester (**5**) and investigated their phototoxicity against melanoma B16-F10 and A375 cells because melanoma is a kind of malignant tumor with increasing incidence and high mortality and therapeutic effects of clinically available drugs (*e.g.* dacarbazine and carmustine) are far from ideal.[33-35] *In vitro* and *in vivo* photodynamic antitumor assays highlighted **7b** as a promising PS for PDT treatment of melanoma. Moreover, the subcellular location as well as the mode of cell death induction of **7b** was clarified by biological assays.

■ RESULTS AND DISCUSSION

1. Synthesis. The synthetic route of the amino acid conjugates (**7**) is shown in **Scheme 1**. Pheophorbide *a* (**1**) was prepared via 36% aqueous HCl degradation of chlorophyll *a* in Et_2O by using our previously established protocol.[36] Treatment of **1** in Et_2O with KOH and *i*-PrOH under an atmosphere of O_2 gave purpurin-18 (**2**) in 34.4% yield.[36] 15-Anhydride ring of **2** was hydrolyzed in the presence of tetrahydrofuran (THF) and CH_3OH using NaOH as the base. The resulting chlorin p_6 (**3**) was rapidly methylated in Et_2O with CH_2N_2 to gave chlorin p_6 trimethylester (**4**) in 83.6% yield.[37] Selective hydrolysis of **4** in THF with 25% aqueous HCl produced **5** in 81.8% yield. The 17^3-carboxylic acid of **5** was activated using 1-hydroxybenzotriazole (HOBt) and 1-ethyl-3-(3-dimethylaminopropyl)-carbodiimide hydrochlorate (EDCI) and coupled individually with *L*-glutamic acid di-*tert*-butyl ester hydrochlorate and *L*-aspartic acid di-*tert*-butyl ester hydrochlorate in N,N-diisopropylethylamine (DIPEA) to form its *tert*-butyl-protected glutamyl (**6a**) and aspartyl (**6b**) derivatives, which were followed by deprotection with trifluoroactic acid (TFA) to afford the target compounds glutamylchlorin p_6 dimethyl ester (**7a**) or **7b** in 61.9% and 58.0% yields, respectively.

Scheme 1[a]

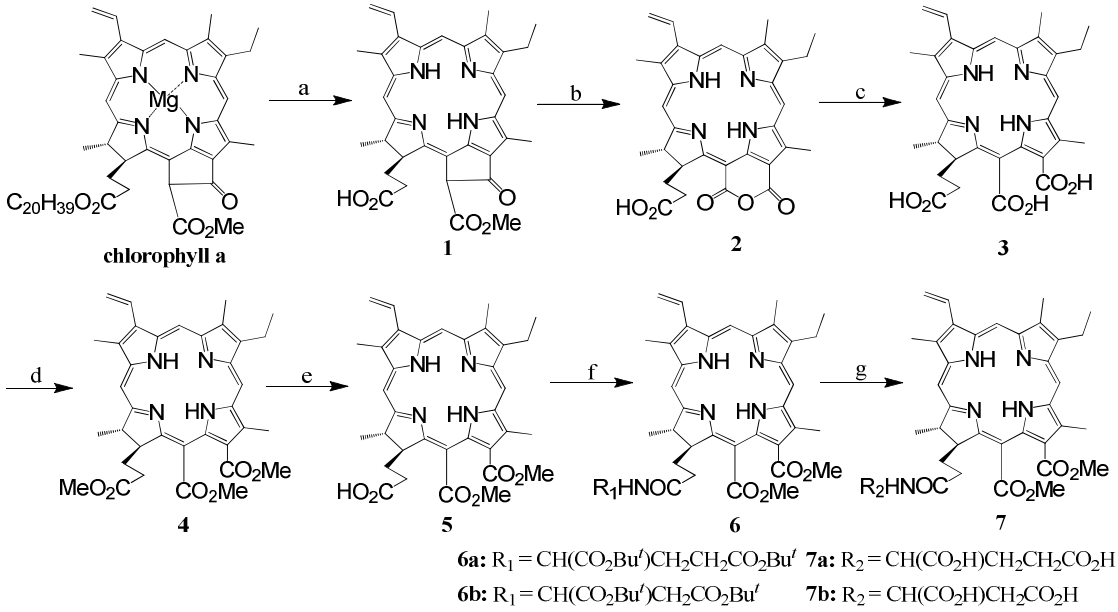

[a] Reagents and Conditions: (a) 36% HCl, Et_2O, 5~10 °C, 30 min; (b) KOH, *i*-PrOH, O_2, 12 h, 34.4%; (c) THF-CH_3OH (1:4), 0.5 M NaOH, rt, 3 h (d) CH_2N_2, rt, 5 min, two steps (c→d) 83.6%; (e) THF-25% aqueous HCl (1:1), rt, 4 h, 81.8%; (f) L-Glu(OBu^t)$_2$ •HCl

or L-Asp(OBu^t)$_2$•HCl, EDCI, HOBt, DIPEA, CH_2Cl_2, rt, 12 h; (g) CH_2Cl_2-TFA (3:1), rt, 6 h; two steps (f→g) 61.9% (**7a**) and 58.0% (**7b**).

Scheme 2[a]

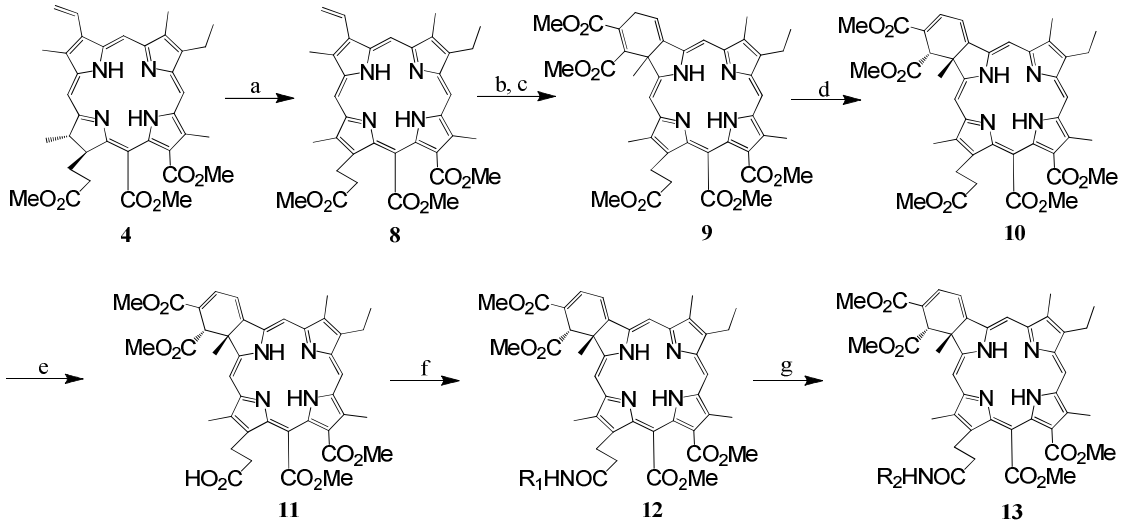

[a] Reagents and Conditions: (a) DDQ, CH_2Cl_2-toluene (6:1), rt, 30 min, 53.5%; (b) DMAD, toluene, microwave 3 h; (c) DMAD, toluene, reflux, 24 h, two steps (b→c) 42.3%; (d) DBU, CH_2Cl_2, rt, 30 min, 94.9%; (e) THF-25% aqueous HCl (1:1), rt, 2.5 h, 96.8%; (f) EDCI, HOBt, L-Glu(OBu^t)$_2$•HCl or L-Asp(OBu^t)$_2$•HCl, DIPEA, CH_2Cl_2, rt, 12 h; (g) CH_2Cl_2-TFA (3:1), 6 h, two steps (f→g) 75.1% (**13a**) and 62.7% (**13b**).

The synthesis of the amino acid conjugates (**13**) of **11** is outlined in **Scheme 2**. Oxidation of **4** by 2, 3-dichloro-5, 6-dicyano-1, 4-benzoquine (DDQ) in toluene produced chloroporphyrin p_6 trimethylester (**8**) in 53.5% yield.[27] Microwave reaction of **8** with dimethyl acetylenedicarboxylate (DMAD) in toluene for 3 h followed by refluxing for 24 h afforded the Diels-Alder adduct (**9**) in 42.3% yield. Compared to the procedure of Zhang *et al*.,[27] the reaction time was greatly shortened from 6 d to 27 h under the microwave condition. Rearrangement of **9** with 1,8-diazabicyclo[5.4.0]undec-7-ene (DBU) formed benzochloroporphyrin p_6 trimethylester *cis*-isomer (BCPD-18, **10**) in 94.9% yield and selective 17^3-ester hydrolyzation of **10** by 25%

aqueous HCl provided **11** in 96.8% yield.[27] The 17-carboxylic acid of **11** was activated using HOBt and EDCI and coupled individually with *L*-glutamic acid di-*tert*-butyl ester hydrochlorate and *L*-aspartic acid di-*tert*-butyl ester hydrochlorate in DIPEA to obtain its *tert*-butyl-protected glutamyl (**12a**) or aspartyl (**12b**) derivatives, which were followed by deprotection in CH_2Cl_2 with TFA to afford the target compounds glutamyl BCPD-18MA (**13a**) and aspartyl BCPD-18MA (**13b**) in 75.1% and 62.7% yields, respectively.

2. Photophysical properties and water solubility. As shown in **Table 1**, UV-visible spectra of the amino acid conjugates **7a**, **7b**, **13a** and **13b** showed the long wavelength absorption maxima in visible bands at 666, 667, 675 and 675 nm, respectively. They exhibited stronger absorption at long wavelength than corresponding lead compounds **5** and **11**. Among them, **7b** possessed the largest molar absorption coefficient at long wavelength of 667 nm.

Moreover, the UV absorption spectra (**Figure 1A**), the time-resolved fluorescence (**Figure 1B**) and $^1O_2$ luminescence spectra (**Figure 1C**) of **5**, **7a** and **7b** were determined. The lifetimes of fluorescence and $^1O_2$ could be derived by fitting the corresponding spectra (**Figure 1D**) and the results indicated that the $^1O_2$ luminescence intensities of **5**, **7a**, **7b** and Al(III)phthalocyanine chloride tetrasulfonic acid (AlPcS) showed a linear dependence on their absorbance. The data gave an excellent fit to a straight line with zero intercept, and the slope of the line was predicted by the computational fit. The determination of $^1O_2$ quantum yields was performed for three independent measurements with a maximum standard deviation of 5%. As summarized in **Table 2**, no significant differences were observed for the lifetimes of fluorescence, $^1O_2$ and triplet-state among **5**, **7a** and **7b**, while the $^1O_2$ quantum yield of **7b** was 2-fold of the standard control AlPcS. As compared to **5** and **7a**, **7b** could be a potential PS for PDT with higher $^1O_2$ quantum yield. The $^1O_2$ lifetimes (10.4 ± 0.4 μs) of **5**, **7a** and **7b** in methanol were agreed well with the value obtained by Young *et al*.[38] In addition, the water solubility of **5** and **7b** was determined by our reported protocol.[39] As expected, the aqueous solubility of **7b** (solubility: 41.7 μM) was

significantly better than its lead compound **5** (water solubility: < 1.6 μM).

Table 1. UV-vis Data for Lead Compounds (5, 11) and Their Corresponding Amino Acid Conjugates

Compounds	λ_{max} (CH_3OH, nm) ($\varepsilon \times 10^4$, M^{-1} cm^{-1})				
	Soret band	Visible bands			
5	397 (34.7)	497 (6.22)	529 (2.31)	612 (2.23)	667 (17.3)
7a	399 (48.1)	497 (8.92)	528 (5.39)		666 (27.2)
7b	398 (61.5)	497 (10.1)	529 (6.14)	612 (5.46)	667 (37.3)
11	431 (7.91)			582 (1.93)	674 (1.50)
13a	437 (9.41)			583 (2.44)	675 (1.86)
13b	435 (8.97)			581 (3.49)	675 (2.81)

Table 2. Fluorescence Lifetime, $^1O_2$ Lifetime, Triplet-state Lifetime and $^1O_2$ Quantum Yield for Lead Compound (5) and its Amino Acid Conjugates

Compounds	$\tau_{fluorescence}$ (ns)	$\tau_{Singlet\ Oxygen}$ (μs)	$\tau_{triplet}$ (μs)	$\Phi_{Singlet\ Oxygen}$
5	3.52	10.98	0.19	0.43
7a	3.45	10.36	0.17	0.30
7b	3.48	10.21	0.18	0.59

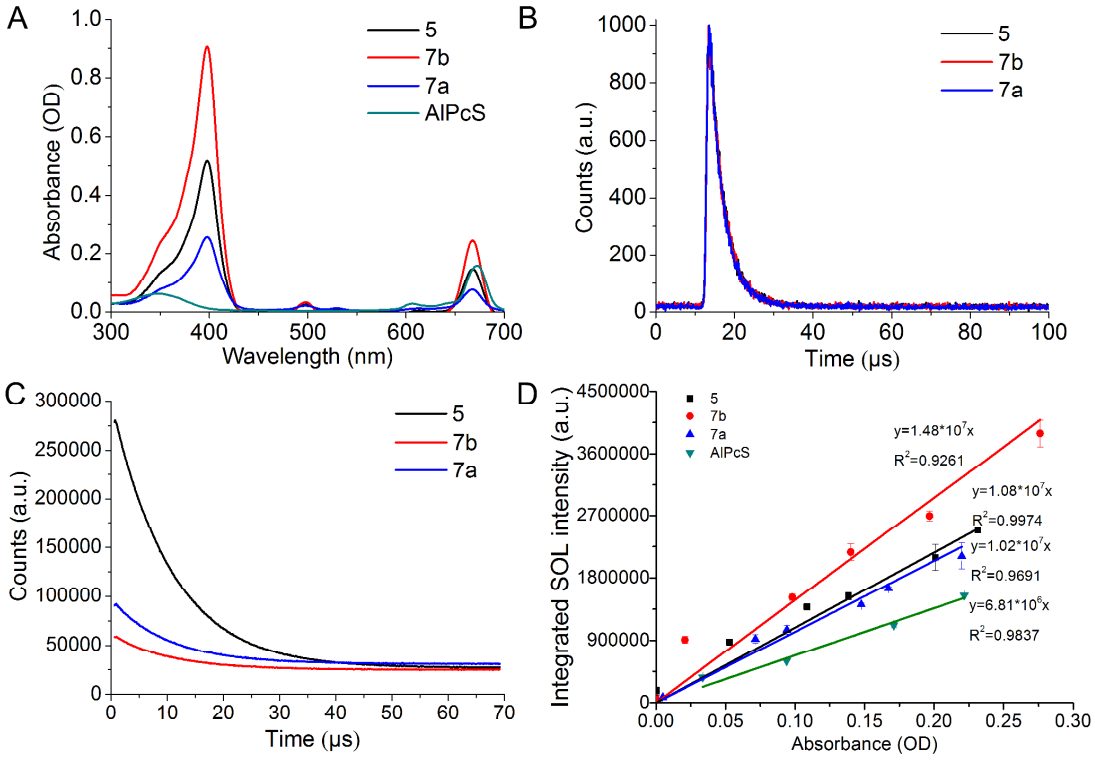

Figure 1. Photophysical properties of the target compounds. (A) UV absorption spectra of **5**, **7a**, **7b** and AlPcS in methanol; (B) The

time-resolved fluorescence of **5**, **7a**, **7b**; (C) $^1O_2$ luminescence spectra (λ_{ex} = 532 nm) of **5**, **7a**, **7b**; (D) Plot of $^1O_2$ luminescence counts against the absorbance for **5**, **7a**, **7b** and AlPcS in methanol. The error bars represent the standard deviation of the mean of three independent measurements.

3. Cytotoxicity. An effective PS needs to possess high phototoxicity and low dark-toxicity, which is measured as the dark-toxicity/phototoxicity ratio. The dark-toxicity and phototoxicity of the amino acid conjugates **7a**, **7b**, **13a**, **13b** as well as their corresponding lead compounds **5** and **11** were evaluated in melanoma B16-F10 and A375 cells exposed to various concentrations of each compound using the cell-counting kit-8 (CCK-8) assay.

As shown in **Table 3**, compared to lead compounds **5** and **11**, target conjugates **7a**, **7b**, **13a** and **13b** exhibited higher dark-toxicity/phototoxicity ratio although both dark-toxicity and phototoxicity was decreased. Among them, **7b** showed the lowest dark-toxicity against both B16-F10 and A375 cells with IC_{50} larger than 300 μM, which was more than 8.3-fold lower than verteporfin. Interestingly, after exposure to light (10 J/cm^2), all the conjugates were found to be highly toxic to B16-F10 and A375 cells, and the phototoxicity of aspartic acid conjugates **7b** and **13b** was better than that of the corresponding glutamic acid conjugates **7a** and **13a**, which was consistent well with the result that **7b** had higher $^1O_2$ quantum yield than **7a**. Moreover, **7b** was the most phototoxic compound, which was more potent than verteporfin.

Table 3. Cytotoxicity for Lead Compounds (5, 11) and Their Corresponding Amino Acid Conjugates against B16-F10 and A375 cells Using CCK-8 Assay

Compounds	B16-F10			A375		
	dark-toxicity (IC_{50}, μM)	phototoxicity (IC_{50}, μM)	ratio	dark toxicity (IC_{50}, μM)	phototoxicity (IC_{50}, μM)	ratio
5	15.67	0.30	52.23	31.33	0.52	60.25
7a	284.20	1.22	232.95	> 300	1.54	> 194.81
7b	> 300	0.68	> 441.18	> 300	0.98	> 306.12
11	15.33	0.92	16.66	22.77	1.47	15.49
13a	224.40	4.06	55.27	286.20	7.10	40.31

13b	271.20	2.29	118.43	> 300	3.02	> 99.34
verteporfin	24.92	1.20	20.77	36.33	2.06	17.64

In order to further confirm the reliability of the obtained results, the survival fraction of B16-F10 and A375 cells treated by **5**, **7a, 7b** and verteporfin under dark or light irradiation at dosage of 10 J/cm^2 were measured at various concentrations. As shown in **Figure 2**, the conjugates **7a** and **7b** had far lower dark-toxicity than lead compound **5**, and their phototoxicities were in a good drug-dose dependent manner. In addition, the phototoxicity of the most phototoxic compound **7b** with various light dosages at a concentration of 5 μM was also determined in order to validate the rationality of light dosage used in all above phototoxicity assays. As shown in **Figure 3**, the phototoxicity of compound **7b** correlated well with light dose within a certain range, and the light dose of 10 J/cm^2 was really appropriate for the above phototoxicity measurement. Moreover, the dark-toxicity and phototoxicity of **7b** and verteporfin against B16-F10 cells was further validated using the MTT assay (**Figure 4** and **Table 4**). As expected, the phototoxicity of **7b** was also in a good drug-dose dependent manner. As shown in **Table 3** and **Table 4**, similar dark-toxicity and phototoxicity of **7b** and verteporfin were obtained in both CCK-8 assay and MTT assay. Taken together, all the results suggested that **7b** might be a promising PS for the PDT applications because it has the highest dark-toxicity/phototoxicity ratio (> 400 for B16-F10 cells and > 306 for A375 cells). Thus, *in vivo* PDT antitumor efficacy and mechanism for **7b** were further investigated.

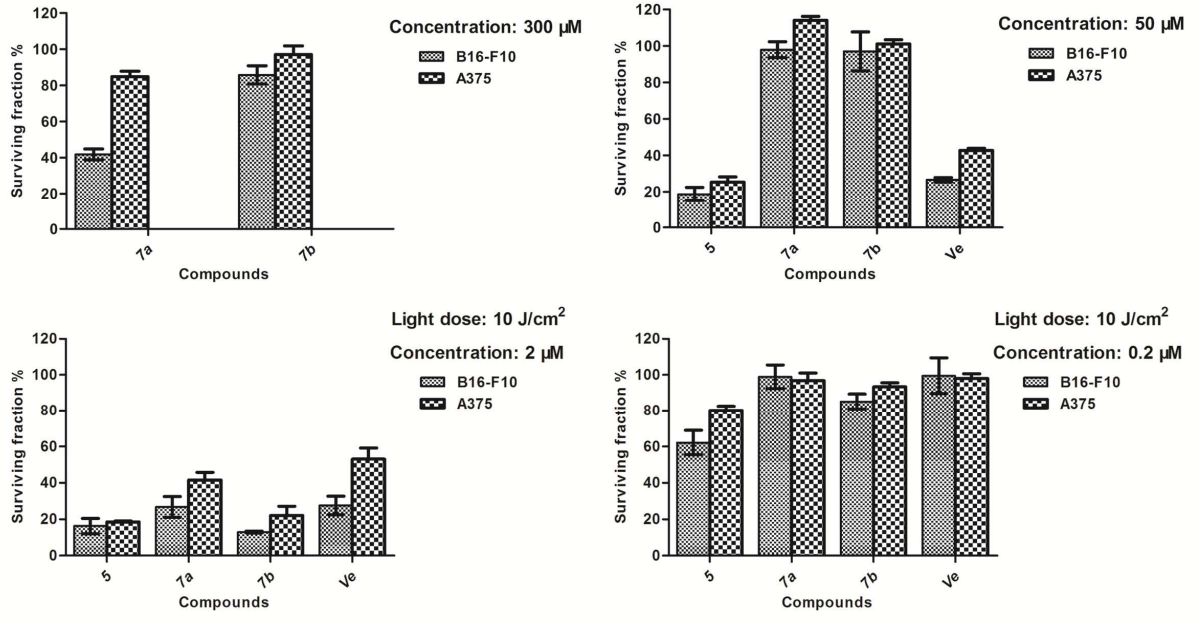

Figure 2. Survival fraction of B16-F10 and A375 cells treated by **5**, **7a**,**7b** and verteporfin ("ve") at the concentrations of 300 μM and 50 μM under dark or at the concentrations of 2 μM and 0.2 μM with a light dose of 10 J/cm^2 using the CCK-8 assay.

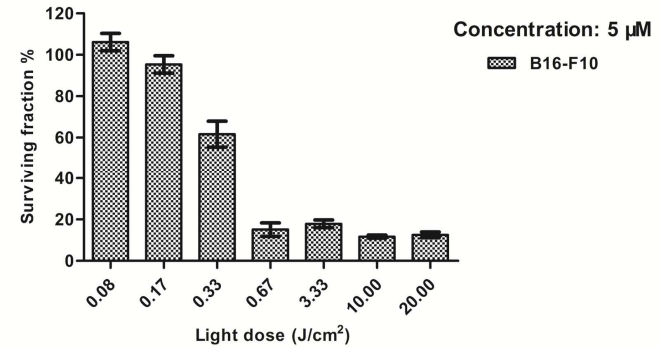

Figure 3. Survival fraction of B16-F10 cells treated by 7**b** with various light dosages at the concentration of 5 μM using the CCK-8 assay.

Table 4. Cytotoxicity for Compound 7b and Verteporfin against B16-F10 Cells Using the MTT Assay

Compounds	dark-toxicity (IC_{50}, μM)	phototoxicity (IC_{50}, μM)	ratio
7b	> 300	0.75	> 400.0
verteporfin	25.03	1.07	23.39

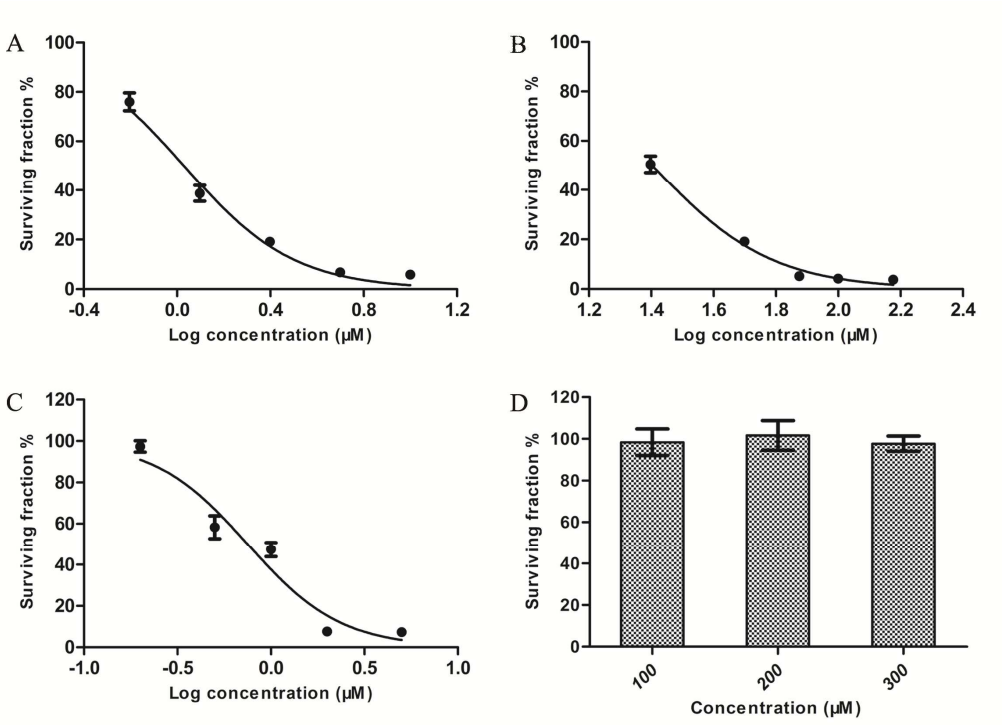

Figure 4. *In vitro* phototoxicity of verteporfin (A), **7b** (C) and dark-toxicty of verteporfin (B), **7b** (D) toward B16-F10 cells using the MTT assay.

4. Subcellular localization. The subcellular localization of the PS is of special significance, since it determines the site of primary photodamages and the type of cellular response to the therapy. While the ROS, especially $^1O_2$, is short-lived, its intracellular targets are close to the sites where the PS is located. Therefore, cellular structures containing PS would be preferentially damaged upon illumination.[13, 40, 41]

The preferential sites of subcellular localization of conjugate **7b** were evaluated by laser confocal microscopy upon exposure of B16-F10 cells to **7b** (10 μM) for 24 h. **Figure 5** showed the fluorescent pattern observed for **7b** and its overlay with the organelle specific fluorescent probes Lyso Tracker Green (lysososomes), Mito Tracker Green FM (mitochondria), Golgi Tracker Green (golgi apparatus), and ER Tracker Green (endoplasmic reticulum). The images were obtained by merging the fluorescence of Lyso Tracker Green DND-26 (green signal, **Figure 5G**), Mito Tracker Green FM (green signal, **Figure 5C**), Golgi Tracker Green (green signal, **Figure 5K**), and ER Tracker Green (green signal, **Figure 5O**) with that of **7b** (red signal, **Figures 5B**, **5F**, **5J** and **5N**). After entry into

cells, **7b** was not observed inside the nucleus of B16-F10 cells.

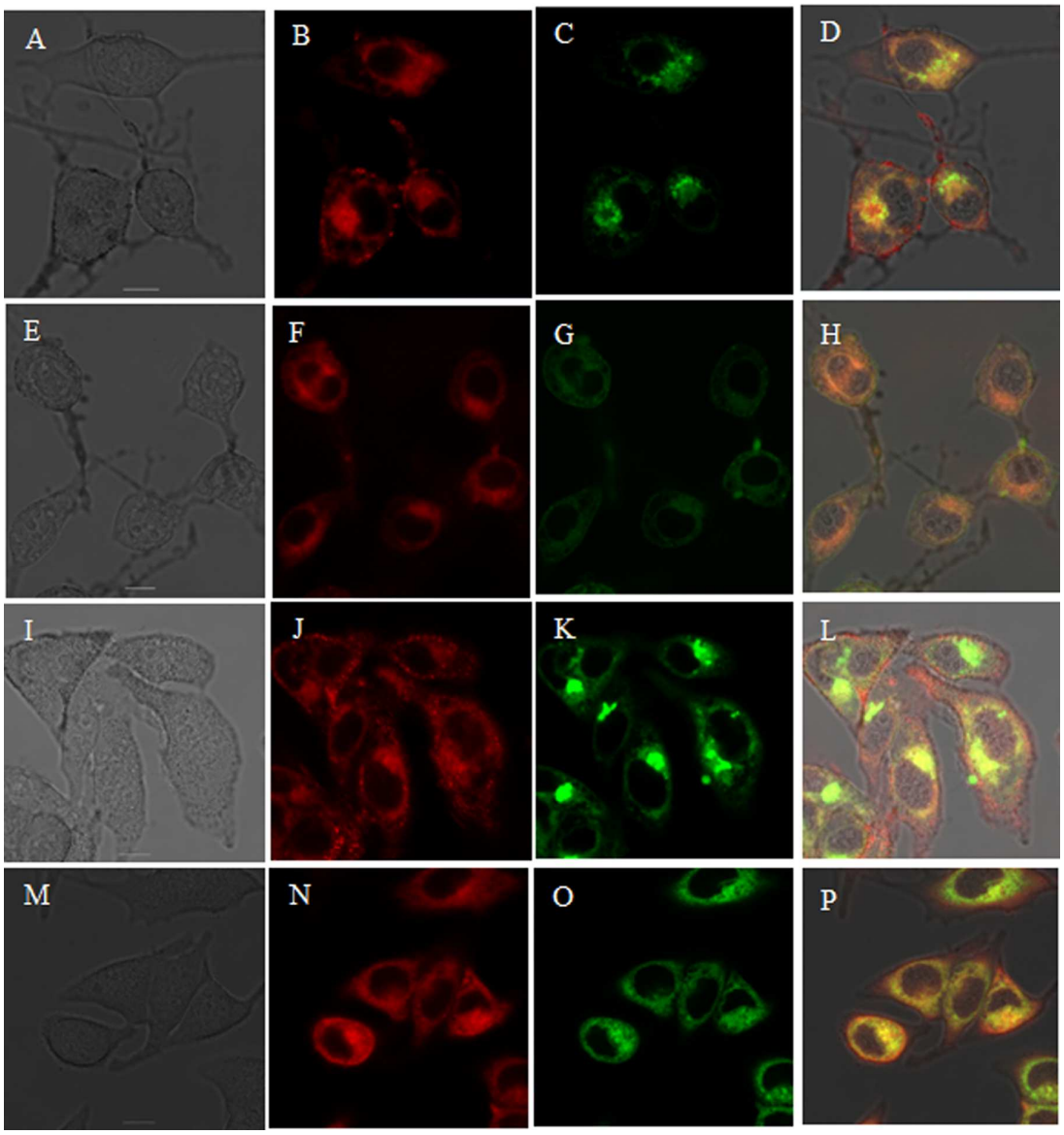

Figure 5. Subcellular location of **7b** in B16-F10 cells at 10 μM for 24 h: (A, E, I, M) phase contrast; (B, F, J, N) red fluorescence corresponds to **7b**; (C) Mito Tracker Green fluorescence; (G) Lyso Tracker Green fluorescence; (K) Golgi Tracker Green fluorescence; (O) ER Tracker Green fluorescence; (D, H, L, P) overlays of organelle trackers with **7b** fluorescence. Scale bar: 10 μm.

The merged stained images revealed the overlaps of **7b** with Mito Tracker Green FM (yellow signal, **Figure 5D**), Lyso Tracker Green DND-26 (yellow signal, **Figure 5H**), Golgi Tracker Green (yellow signal, **Figure 5L**), and ER Tracker Green (yellow signal, **Figure 5P**), suggesting that mitochondria, lysosomes, Golgi, and ER were

all the sites of its intracellular distribution. Mitochondria were the most important cell organs related to apoptosis and also exhibited peripheral benzodiazepine receptor (PBR) binding, which might be an important target for PDT.[42-44] Photodamage to lysosomes could inhibit autophagy, a potentially cyto-protective effect. Therefore, the loss of autophagy could improve the overall photodynamic effect in cells capable of initiating an apoptotic program in response to photodamage.[6, 45] ER is one of the most critical sites for PDT and also could induce apoptosis. Thus, localization in ER could lead to activation of apoptotic pathways. In addition, the localization in ER could also cause photodamage to Bcl-2 or release of cytochrome C with pro-apoptotic consequences.[6, 46] Presumably, the photodamage effect to multiple organelles caused by **7b** could trigger various apoptotic pathways, leading to effective cell destruction.[47, 48]

5. Determination of the apoptotic cell death *in vitro*. Many excited PS generate ROS that lead to induction of apoptosis in malignant cells.[27,49-51] Nuclear fragmentation and phosphatidylserine exposure were studied to evaluate the effects of **7b** on inducing cell apoptosis. The redistribution of plasma membrane phosphatidylserine is an early marker of apoptosis. Since Annexin V-FITC can also be used to detect necrotic cells as a result of the loss of membrane integrity, apoptotic cells are differentiated from necrotic cells by an increase in PI (propidium iodide) positivity, which selectively labels necrotic but not apoptotic cells. To monitor the concentration gradient of phosphatidylserine exposure, Annexin V-FITC binding and PI uptake were measured by flow cytometry. As shown in **Figure 6**, the significant increase in both Annexin V-FITC binding and PI uptake was observed at 24 h post-irradiation at a dose of 2 μM (**Figure 6B**) or 5 μM (**Figure 6C**). The results indicated that **7b** could mainly cause both cell necrosis and cell late period apoptosis in a dose dependent manner. The result was consistent with the fact that **7b** was localized in multiple subcellular organelles such as mitochondria, lysosomes, golgi apparatus and ER (**Figure 5**).

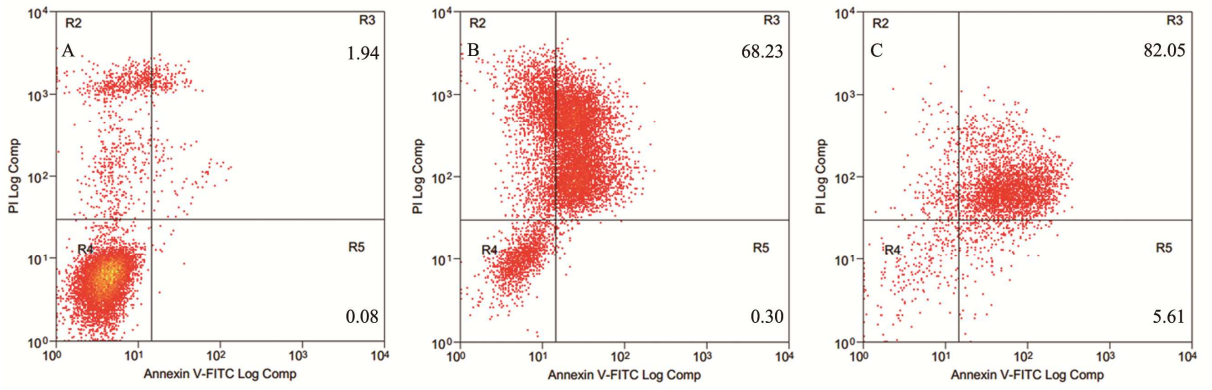

Figure 6. Flow cytometry analysis of B16-F10 cells with Annexin V/PI double staining after PDT: (A) Blank; (B) Treated with 2.0 μM of **7b** at a light dose of 10 J/cm^2; (C) Treated with 5.0 μM of **7b** at a light dose of 10 J/cm^2. UL (upper left quadrant), Annexin V (-) PI (+), cell fragment; UR (upper right quadrant), Annexin V (+) PI (+), necrosis or the late period apoptosis; LL (lower left quadrant), Annexin V (-) PI (-), survival cell; LR (lower right quadrant), Annexin V (+) PI (-), early period apoptosis

6. *In vivo* photodynamic antitumor potency. PDT antitumor efficacy of **7b** on C57BL/6 mice bearing B16-F10 tumor was evaluated. As illustrated in **Figures 7** and **8**, the growth of the implanted tumors in **7b**-PDT group (1 mg/kg), and verteporfin-PDT group (2 mg/kg, positive control) was significantly inhibited compared to negative control group ($P < 0.05$), and no significant difference was found among **7b**-PDT group (1 mg/kg) and verteporfin-PDT group (2 mg/kg) ($P > 0.05$). Furthermore, Kaplan-Meier analysis also showed that compare to negative control group (median survival = 13 d), the survival times of **7b**-PDT group (median survival = 21 d) and verteporfin-PDT group (median survival = 18 d) were both significantly prolonged ($P < 0.05$), while **7b**-PDT group and verteporfin-PDT group also showed no significant difference ($P > 0.05$) on the survival time. Overall, these results demonstrated that the *in vivo* antitumor potency of **7b** at dose of 1 mg/kg was comparable to that of verteporfin at dose of 2 mg/kg, indicating that **7b** might possess more potent PDT antitumor efficacy at equal doses. It should be noted that verteporfin was in liposome form and could selectively accumulate at tumor site by EPR (enhanced permeability and retention) effect,[52] and **7b** was in form of water-soluble sodium salt. The preparation of **7b** in a better formulation such also as liposome might result in better *in vivo* antitumor potency.

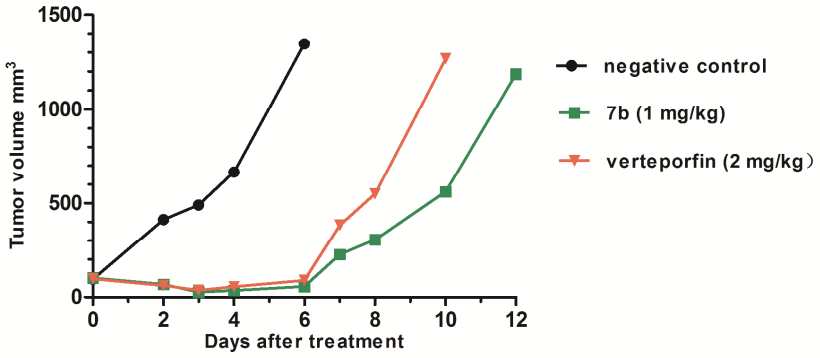

Figure 7. PDT efficacy on C57BL/6 mice bearing B16-F10 tumor. The mice were divided into 3 groups (5 mice in each group): negative control (black line), **7b**-PDT (1 mg/kg, green line), verteporfin-PDT (2 mg/kg, red line). The tumors were irradiated with laser light (678 nm, 150 J/cm^2) at 2 h after intravenous administration.

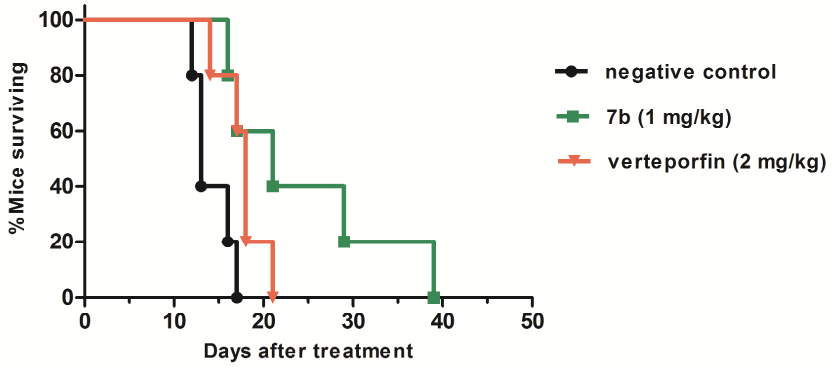

Figure 8. Kaplan-Meier survival curve of C57BL/6 mice bearing B16-F10 tumor. $P < 0.05$ for verteporfin-PDT group and **7b**-PDT group, compared with negative control by log-rank test ($n = 5$).

■ CONCLUSIONS

In summary, we designed and synthesized a series of novel chlorin p_6-based water-soluble amino acid conjugates containing glutamic acid and aspartic acid residues using Chinese traditional herb silkworm excrement as the starting material. The target conjugates **7a**, **7b**, **13a** and **13b** exhibited higher *in vitro* dark-toxicity/phototoxicity ratio against melanoma B16-F10 and A375 cells compared to corresponding lead compounds **5** and **11**. Among them, **7b** showed the highest phototoxicity and the lowest dark-toxicity, which was

even more phototoxic and less dark-toxic than verteporfin. It also exhibited better *in vivo* photodynamic antitumor efficacy on C57BL/6 mice bearing B16-F10 tumor than verteporfin (in liposome formulation). In addition, **7b** was found to localize in multiple subcellular organelles including lysosomes, mitochondria, golgi apparatus and endoplasmic reticulum (ER), and could cause both cell necrosis and apoptosis after PDT in a dose dependent manner, leading to more effective cell destruction. Taken together, our data support the fact that **7b** is a promising PS for PDT applications due to its strong absorption in the phototherapeutic window (λ_{max} = 667 nm, ε = 3.73 $\times 10^5$ M^{-1} cm^{-1}), relatively high $^1O_2$ quantum yield, hightest dark-toxicity/phototoxicity ratio (> 400 for B16-F10 cells and > 306 for A375 cells), good water-solubility and excellent *in vivo* PDT antitumor efficacy. Further evaluation of PS candidate **7b** for clinical trial was in progress.

■ EXPERIMENTAL SECTION

1. Chemistry. All chemicals were of regent grade. All air and moisture sensitive reactions were performed in dried solvents under a nitrogen atmosphere. All solvents and reagents were purchased from commercial sources, unless otherwise stated. Thin-layer chromatography (TLC) analysis was carried out on silica gel plates GF_{254} (QindaoHaiyang Chemical, China). Silica gel column chromatography was performed with Silica gel 60G (QindaoHaiyang Chemical, China). ^1H and ^{13}C spectra were recorded on Bruker MSL-300 or MSL-600 or Varian Unity Inova-500 spectrometers, with TMS as the internal standard and $CDCl_3$ or CD_3OD or $(CD_3)_2SO$ (DMSO-d_6) as the solvents. Chemical shifts (δ) and coupling constants (*J*) are given in ppm and Hz, respectively. ESI mass spectrometric data were collected on an API-3000 LC-MS spectrometer or a Micromass Qtof-Micro LC-MS-MS. UV absorption spectra were measured on an Agilent UV 8453 or Techcomp UV 1102 spectrophotometers. Purity of the target compounds were analyzed by high performance liquid chromatography (HPLC) (Agilent Technologies 1260 Infinity) using MeOH / THF / H_2O / HOAc (30:25:44.5:0.5, volume ratio) of 1 mL / min on a C18 column (Aglilent 20RBA × SB-C18, 5 μm, 4.6 mm × 150 mm). All compounds exhibited more than 95%

purity. All solvents and regents were analytically pure, and no further purification was needed. All starting materials were commercially available.

*Chlorin p_6 dimethylester (**5**)*. **4** (375 mg, 0.601 mmol), which was synthesized as previously reported.[36,37], was dissolved in THF (100 mL) with addition of 25% HCl aqueous solution (100 mL). The mixture was stirred at room temperature for 4 h. The reaction mixture was diluted with water and adjusted to pH 5~6 with aqueous sodium hydroxide and then extracted with CH_2Cl_2. The organic layer was washed with water, dried over anhydrous Na_2SO_4, and evaporated. The residue was dissolved in CH_2Cl_2 and purified on a silica gel column (3% methanol in CH_2Cl_2 as eluent) to afford 300 mg, 0.492 mmol, 81.8% yield of **5** ($C_{35}H_{38}N_4O_6$). MS (ESI^+) *m/z*: 611.39 $[M+H]^+$ (100%). UV-vis λ_{max} (CH_3OH, nm) (ε / $M^{-1}cm^{-1}$): 667 (1.73×10^5), 610 (2.23×10^4), 529 (2.31×10^4), 497 (6.22×10^4), 397 (3.47×10^5). ^1H NMR [$CDCl_3$, 600 MHz]: δ 9.69 (s, 1H), 9.47 (s, 1H), 8.66 (s, 1H), 7.95 (dd, J = 18.0, 11.4 Hz, 1H), 6.29 (d, J = 18.0 Hz, 1H), 6.12 (d, J = 11.4 Hz, 1H), 5.16 (m, 1H), 4.39 (m, 1H), 4.20 (s, 3H), 4.14 (s, 3H), 3.71 (m, 2H), 3.64 (s, 3H), 3.38 (s, 3H), 3.23 (s ,3H), 2.43-2.10 (m, 4H), 1.85 (d, J = 6.0 Hz, 3H), 1.69 (t, J = 7.8 Hz, 3H), -1.0 (br s, 2H). HPLC purity: 98.8%.

*Glutamylchlorin p_6 dimethylester (**7a**)*. **5** (110 mg, 0.180 mmol) was dissolved in anhydrous CH_2Cl_2 (30 mL). EDCI (41.5 mg, 0.216 mmol, 1.2 equiv.) and HOBt (29.2 mg, 0.216 mmol l, 1.2 equiv.) were then added and allowed to stir until completely dissolved under argon in ice-salt bath. After 30 min, L-Glu(OBu^t)$_2$•HCl (60.9 mg, 0.216 mmol l, 1.2 equiv.) and DIPEA (0.038 mL, 0.216 mmol l, 1.2 equiv.) were mixed in CH_2Cl_2 (10 mL) and added to the reaction mixture. The mixture was allowed to stir at room temperature overnight under nitrogen. It was diluted with CH_2Cl_2 (200 mL) and then washed with 5% aqueous citric acid, brine and water, respectively. The organic layer was dried over anhydrous Na_2SO_4 and evaporated. The residue was dissolved in dry CH_2Cl_2/TFA (3:1, 15 mL) and stirred at room temperature for 6 h. The resulting mixture was diluted with CH_2Cl_2 and adjusted to pH 3~4 with 10% $NaHCO_3$ and purified on a silica gel column (5% CH_3OH in CH_2Cl_2 as eluent) to give 82.5 mg, 0.112 mmol, 61.9% yield of **7a** ($C_{40}H_{45}N_5O_9$). MS (ESI^+) *m/z*: 740.42 $[M+H]^+$ (100%). UV-vis

λ_{max} (CH_3OH, nm) (ε / $M^{-1}cm^{-1}$): 666 (2.72×10^5), 528 (5.39×10^4), 497 (8.92×10^4), 397 (4.81×10^5). ^{1}H NMR [$(CD_3)_2SO$, 600 MHz]: δ 12.33 (br s, 2H)), 9.67 (s, 1H), 9.45 (s, 1H), 8.98 (s, 1H), 8.10 (dd, *J* = 18, 12 Hz, 1H), 8.03 (d, *J* = 12 Hz, 1H), 6.34 (d, *J* = 18 Hz, 1H), 6.10 (d, *J* = 12 Hz, 1H), 4.99 (m, 1H), 4.58 (m, 1H), 4.15 (s, 3H), 4.12 (s, 3H), 3.98 (m, 2H),3.56 (s, 3H), 3.40 (s ,3H), 3.38 (m, 1H), 3.09 (s, 3H), 2.28 (m, 2H), 2.18 (m, 2H), 2.01 (m, 2H), 1.88 (m, 2H), 1.83 (d, *J* = 6.0 Hz, 3H), 1.65 (t, *J* = 6.0 Hz, 3H), -1.14 (s, 1H), -1.29 (s, 1H). ^{13}C NMR [$(CD_3)_2SO$, 600 MHz]: δ 173.59, 173.42, 173.30, 171.74, 169.75, 167.27, 166.09, 154.16, 148.17, 144.95, 140.56, 137.28, 136.03, 135.11, 134.20, 131.19, 128.76, 128.66, 122.63, 122.53, 104.22, 103.13, 99.79, 94.13, 52.79, 52.62, 52.29, 51.10, 48.16, 32.43, 31.53, 30.01, 28.89, 26.22, 23.49, 18.54, 17.51, 12.00, 11.85, 10.64. HRMS (ESI^+) *m/z*: 740.3290 $[M + H]^+$, calcd for $C_{40}H_{46}N_5O_9$ 740.3217. HPLC purity: 97.6%.

Aspartylchlorin p_6 dimethylester (***7b*)**. **5** (120 mg, 0.197 mmol) was reacted with L-Asp(OBu^t)$_2$•HCl (66.4 mg, 0.237 mmol, 1.2 equiv.) by following the procedure for the synthesis of **7a** to obtain 82.7 mg, 0.114 mmol, 58.0% yield of **7b** ($C_{39}H_{43}N_5O_9$). MS (ESI^+) *m/z*: 726.43 $[M+H]^+$ (100%). UV-vis λ_{max} (CH_3OH, nm) (ε / $M^{-1}cm^{-1}$): 667 (3.73×10^5), 612 (5.46×10^4), 529 (6.14×10^4), 497 (1.01×10^5), 398 (6.15×10^5). ^{1}H NMR [$(CD_3)_2SO$, 600 MHz]: δ 9.48 (s, 1H), 9.19 (s, 1H), 8.95 (s, 1H), 8.05 (d, *J* = 7.2 Hz, 1H), 7.89 (dd, *J* = 18, 12 Hz, 1H), 6.17 (d, *J* = 18 Hz, 1H), 5.96 (d, *J* = 12 Hz, 1H), 5.01 (m, 1H), 4.61 (m, 1H), 4.45 (m, 1H), 4.17 (s, 3H), 4.16 (s, 3H), 3.51 (s, 3H), 3.36 (m, 1H), 3.31 (s, 3H), 2.88 (s, 3H), 2.61 (m, 1H), 2.49 (s, 2H), 2.35 (m, 1H), 2.09 (m, 3H), 1.84 (d, *J* = 6.6 Hz, 3H), 1.44 (t, *J* = 7.2 Hz, 3H), -1.25 (s, 1H), -1.33 (s, 1H). ^{13}C NMR [$(CD_3)_2SO$, 600 MHz]: δ 173.37, 172.84, 172.03, 171.24, 169.79, 167.31, 166.13, 154.03, 148.05, 144.73, 140.50, 137.17, 135.81, 134.95, 134.21, 131.05, 128.62, 122.48, 122.39, 104.05, 103.13, 99.61, 94.10, 52.82, 52.69, 52.28, 48.62, 48.18, 37.31, 32.73, 31.64, 28.83, 23.51, 18.41, 17.42, 11.97, 11.77, 10.47. HRMS (ESI^-) *m/z*: 724.2987 $[M - H]^+$, calcd for $C_{39}H_{42}N_5O_9$ 724.3059. HPLC purity: 96.3%.

*BCPD-18MA (**11**)*. **4** (300 mg, 0.481 mmol) was dissolved in dry CH_2Cl_2 (90 mL) and added DDQ (70 mg) which was dissolved in methylbenzene (15 mL). The mixture was stirred for 30 min at room temperature and then

washed with 0.1 M aqueous hydrochloric acid and water, respectively. Organic layer was dried over anhydrous Na_2SO_4 and evaporated. The residue was purified on a silica column to obtain 160 mg, 0.257 mmol, 53.5% yield of **8** ($C_{36}H_{38}N_4O_6$). UV-vis λ_{max} (CH_2H_2, nm) (ε / $M^{-1}cm^{-1}$): 549 (7.3×10^3), 511 (6.0×10^3), 406 (1.0×10^5). ^{1}H NMR [$CDCl_3$, 500 MHz]: δ 10.01 (s, 1H), 9.98 (s, 1H), 9.91 (s, 1H), 8.08 (dd, *J* = 17.9, 11.4 Hz, 1H), 6.24 (d, *J* = 17.9 Hz, 1H), 6.10 (d, *J* = 11.4 Hz, 1H), 4.45 (s, 3H), 4.32 (s, 3H), 4.07 (t, *J* = 8.5 Hz, 2H), 3.99 (q, *J* = 7.7 Hz, 2H), 3.80 (s, 3H), 3.67 (s, 3H), 3.60 (s ,3H), 3.54 (s, 3H), 3.52 (s ,3H), 3.08 (t, *J* = 8.5 Hz, 2H), 1.80 (t, *J* = 7.7 Hz, 3H), -3.78 (s, 1H), -3.82 (s, 1H). **8** (228.4 mg, 0.367 mmol) and DMAD (1 mL) were dissolved in methylbenzene (30 mL) and reacted by microwave under 145℃ for 3 h, followed by refluxing under inert N_2 atmosphere for 24 h. The mixture was evaporated and then purified via gel column chromatography (1% methanol in CH_2Cl_2 as eluent) to afford 118 mg, 0.154 mmol, 42.3% yield of **9** ($C_{42}H_{44}N_4O_{10}$). MS (ESI^+) *m/z*: 765.18 $[M+H]^+$ (100%). UV-vis λ_{max} (CH_2H_2, nm) (ε / $M^{-1}cm^{-1}$): 655 (2.0×10^4), 600 (4.6×10^3), 550 (1.1×10^4), 519 (0.9×10^4), 413 (1.5×10^5). ^{1}H NMR [$CDCl_3$, 300 MHz]: δ 9.74 (s, 1H), 9.26 (s, 1H), 9.16 (s, 1H), 7.39 (m, 1H), 4.37 (s, 3H), 4.23 (s, 3H), 3.96 (s, 3H), 3.90 (s, 3H), 4.05 (m, 2H), 3.94 (q, *J* = 7.6 Hz, 2H), 3.81 (s, 3H), 3.52 (s, 3H), 3.60 (m, 2H), 3.45 (s ,3H), 3.42 (s, 3H), 3.02 (m, 2H), 2.13 (s, 3H), 1.76 (t, *J* = 7.6 Hz, 3H), -2.15 (s, 1H), -2.60 (s, 1H). The Diels-Alder adduct **9** (118 mg, 0.154 mmol) was dissolved it in dry CH_2Cl_2 (100 mL). DBU (1 mL) was added, and stirred for 30 min at room temperature. The reaction mixture was washed with 3% HCl, saturated brine, water, respectively. Organic layer was dried over anhydrous Na_2SO_4 and then evaporated. The residue was purified via gel column chromatography (CH_2Cl_2 as eluent) to afford 112 mg, 0.154 mmol, 94.9% yield of **10** ($C_{42}H_{44}N_4O_{10}$). MS (ESI^+) *m/z*: 765.28 $[M+H]^+$ (100%). UV-vis λ_{max} (CH_2H_2, nm) (ε / $M^{-1}cm^{-1}$): 677 (2.3×10^4), 586 (3.1×10^4), 439 (1.1×10^5). ^{1}H NMR [$CDCl_3$, 300 MHz]: δ 9.74 (s, 1H), 9.30 (s, 1H), 9.02 (s, 1H), 7.82 (d, *J* = 5.7 Hz, 1H), 7.44 (d, *J* = 5.7 Hz, 1H), 5.07 (s, 1H), 4.36 (s, 3H), 4.23 (s, 3H), 3.99 (s, 3H), 3.80 (s, 3H), 3.99~3.91 (m, 4H), 3.52 (s, 3H), 3.44 (s ,3H), 3.39 (s, 3H), 3.04 (m, 2H), 3.0 (s, 3H), 1.79 (s, 3H), 1.75 (t, *J* = 7.6 Hz, 3H), -1.92 (s, 1H), -2.23 (s, 1H). **10** (100 mg, 0.131 mmol) was dissolved in THF (30 mL). 25% HCl aqueous solution (30 mL) was added and

stirred at room temperature for 4 h. The mixture was diluted with CH_2Cl_2 and washed with water. Organic layer was then dried over anhydrous Na_2SO_4 and evaporated. The residue was purified via silica gel column chromatography (2.5% methanol in CH_2Cl_2 as eluent) to afford 95 mg, 0.116 mmol, 96.8% yield of **11** ($C_{41}H_{42}N_4O_{10}$). UV-vis λ_{max} (CH_3OH, nm) (ε / $M^{-1}cm^{-1}$): 674 (1.50×10^4), 582 (1.93×10^4), 431 (7.91×10^4). ^1H NMR (DMSO-d_6, 500 Mz): δ 12.43 (s, 1H), 9.88 (s, 1H), 9.68 (s, 1H), 9.41 (s, 1H), 7.83 (d, *J* = 5.6 Hz, 1H), 7.78 (d, *J* = 5.6 Hz, 1H), 5.34 (s, 1H), 4.25 (s, 3H), 4.15 (s, 3H), 3.97 (q, *J* = 7.5 Hz, 2H), 3.93 (s, 3H), 3.81 (t, *J* = 8.4 Hz, 2H), 3.49 (s, 3H), 3.47 (s, 3H), 3.45 (s ,3H), 2.96 (s, 3H), 2.90 (t, *J* = 8.4 Hz, 2H), 1.79 (s, 3H), 1.71 (t, *J* = 7.5 Hz, 3H), -2.08 (s, 1H), -2.39 (s, 1H). HRMS (ESI^+) *m/z*: 751.2967 $[M]^+$, calcd for $C_{41}H_{43}N_4O_{10}$ 751.2894. HPLC purity: 98.9%.

*Glutamyl BCPD-18MA (**13a**)*. **11** (30 mg, 0.04 mmol) was dissolved in dry CH_2Cl_2 (50 mL). EDCI (9.2 mg, 0.048 mmol, 1.2 equiv) and HOBt (6.6 mg, 0.048 mmol, 1.2 equiv.) were then added and allowed to stir until completely dissolved under argon in ice-salt bath. After 30 min, L-Glu(OBu^t)$_2$•HCl (14.3 mg, 0.048 mmol, 1.2 equiv.) and DIPEA (0.010 mL) were dissolved in CH_2Cl_2 (5 mL) and added to the reaction mixture. The mixture was allowed to stir at room temperature overnight under nitrogen. It was then diluted with CH_2Cl_2 and washed with 5% aqueous citric acid, brine and water, respectively. The organic layer was dried over anhydrous Na_2SO_4 and evaporated. The residue was dissolved in dry CH_2Cl_2/TFA (3:1, 20 mL) and stirred at room temperature for 4 h. The resulting mixture was diluted with CH_2Cl_2 and adjusted to pH 3~4 with 10% $NaHCO_3$ and purified on a silica gel column (5% CH_3OH in CH_2Cl_2 as eluent) to afford 26.4 mg, 0.03 mmol, 75.1% yield of **13a** ($C_{46}H_{49}N_5O_{13}$). MS (ESI^-) *m/z*: 878.33 $[M-H]^+$ (100%). UV-vis λ_{max} (CH_3OH, nm) (ε / $M^{-1}cm^{-1}$): 675 (1.86×10^4), 583 (2.44×10^4), 437 (9.41×10^4). ^1H NMR (CD_3OD, 600 MHz): δ 9.39 (s, 1H), 9.27 (s, 1H), 9.23 (s, 1H), 8.16 (s, 1H), 7.84 (d, *J* = 6.0 Hz, 1H), 7.65 (d, *J* = 6.0 Hz, 1H), 5.18 (s, 1H), 4.38 (s, 3H), 4.24 (s, 3H), 4.14 (m, 1H), 4.02 (q, *J* = 6.0 Hz, 2H), 3.99 (s, 3H), 3.97 (m, 2H), 3.54 (s, 3H), 3.39 (s, 3H), 3.35 (m, 2H), 3.04 (s, 3H), 2.94 (m, 2H), 2.89 (s, 3H), 2.25 (m, 2H), 1.82 (t, *J* = 6.0 Hz, 3H), 1.77 (s, 3H). HRMS (ESI^-) *m/z*: 878.3260 $[M - H]^+$, calcd for

$C_{46}H_{48}N_5O_{13}$ 878.3331. HPLC purity: 95.8%.

*Aspartyl BCPD-18MA (**13b**)*. **11** (26 mg, 0.035 mmol) was reacted with L-Asp(OBu^t)$_2$•HCl (11.8 mg, 0.042 mmol, 1.2 equiv) by following method for the synthesis of **13a** to give 18.8 mg, 0.022 mmol, 62.7% yield of **13b** ($C_{45}H_{47}N_5O_{13}$). MS (ESI^+) *m/z*: 866.51 $[M+H]^+$ (100%). UV-vis λ_{max} (CH_3OH, nm) (ε / $M^{-1}cm^{-1}$): 675 (2.81×10^4), 581 (3.49×10^4), 435 (8.97×10^4). ^1H NMR (CD_3OD, 300 MHz): δ 9.27 (s, 1H), 9.07 (s, 1H), 9.00 (s, 1H), 8.35 (s, 1H), 7.87 (d, *J* = 6.0 Hz, 1H), 7.67 (d, *J* = 6.0 Hz, 1H), 5.23 (s, 1H), 4.44 (s, 3H), 4.30 (s, 3H), 4.09 (m, 1H), 4.07 (s, 3H), 4.01 (q, *J* = 9.0 Hz, 2H), 3.59 (s, 3H), 3.50 (m, 2H), 3.38 (s, 3H), 3.35 (m, 2H), 3.16 (s, 3H), 2.97 (m, 2H), 2.53 (s, 3H), 2.05 (t, *J* = 6.0 Hz, 3H), 1.72 (s, 3H). ^{13}C NMR (CD_3OD, 600 MHz): δ 173.99, 173.05, 171.37, 171.11, 169.60, 167.59, 166.49, 154.87, 154.14, 147.18, 144.26, 143.57, 140.47, 138.51, 137.68, 136.78, 136.02, 134.38, 132.73, 131.96, 131.08, 129.73, 129.39, 124.53, 122.69, 118.59, 114.01, 109.23, 99.12, 93.59, 92.38, 53.16, 52.60, 51.73, 51.44, 50.79, 37.04, 31.60, 30.37, 29.56, 22.77, 22.26, 15.37, 12.98, 11.11. HRMS (ESI^+) *m/z*: 866.3246 $[M + H]^+$, calcd for $C_{45}H_{48}N_5O_{13}$ 866.3174. HPLC purity: 96.6%.

Photophysical study. The determination of $^1O_2$ quantum yield is based on the comparison of $^1O_2$ luminescence counts (λ_{max} = 1270 nm) generated from the photosensitization of Al (III) phthalocyanine chloride tetrasulfonic acid (AlPcS, ΦΔ= 0.27) inmethanol and the samples were tested under the same conditions by using the previously established method.[53] The $^1O_2$ lifetimes can be indirectly derived by fitting the $^1O_2$ luminescence spectra.

Cell lines and culture. B16-F10 cells and A375 cells were originally obtained from the Chinese Academy of Sciences Shanghai Institute of Cell Bank (Shanghai, China). B16-F10 cells were cultured in RPMI 1640 medium (Hyclone, Logan, UT, USA) and A375 cells were cultured in DMEM medium (Hyclone, Logan, UT, USA), supplemented with 2 mg/mL sodium bicarbonate, 4.5 mg/mL glucose, 100 μg/mL streptomycin sulfate, 40 mg/mL gentamicin, 100 U/mL penicillin and 10% (*v/v*) heat-inactivated fetal bovine serum (FBS) in 5% CO_2, 95% air in a humidified incubator at 37℃.

Mouse bearing tumor model. C57BL/6 male mice aged 6-8 weeks with a mean body weight of 22 ± 2 g were purchased from Shanghai SLAC Laboratory Animal Co. Ltd (Shanghai, China). B16-F10 cells (2×10^4) were subcutaneously inoculated into the right thigh of mice. Measurement of the tumor size was started on day 8 after inoculation. Only those mice with tumor diameter between 6 to 8 mm were used. The animals were given free access to food and water during the experiment.

Two parameters (length and width) of the tumor were measured using a micrometer digital caliper (500-157-20, Mitutoyo, Japan). The tumor volume was calculated using the following formula: $V = (W^2 \times L)/2$, according to the US National Cancer Institute protocol, where W is the width and L is the length of the tumor.

Dark cytotoxicity. 5×10^3 cells were seeded on a 96-well culture transwell apparatus (Costar, Cambridge, MA, USA) and cultured in RPMI 1640 medium or DMEM medium with 10% (*v/v*) fetal bovine serum (FBS), respectively. The tested compounds were diluted to different final concentration and the cells were incubated for 48 h in a CO_2 incubator at 37 ℃.

CCK-8 assay. Above loading media were removed, and the cells were fed new medium, followed by 20 μL of Cell Counting Kit-8 (CCK-8) per 200 μL of medium and incubated for 1.5 h. The cell viability was then assessed by Cell-Counting Kit-8 assay (Dojindo Laboratories, Japan) following the manufacturers' protocol. The absorbance of each well was monitored by a spectrophotometer (Tecan, Switzerland) at 450 nm. [54]

MTT assay. Above loading media were removed, and the cells were fed new medium, followed by 20 μL of 3-(4,5-dimethylthiazol-2 yl)-2,5-diphenyl tetrazolium bromide (MTT) per 150 μL of medium and incubated for 4 h. Dimethyl sulfoxide (DMSO) was then used to dissolve the formazan crystals and the absorbance was measured at 490 nm using anspectrophotometer (Tecan, Switzerland). [55]

Phototoxicity. The B16-F10 cells and A375 cells were prepared as described above with the tested compounds of different concentrations and incubated for 24 h in a 5% CO_2 incubator at 37℃. After receiving irradiation with the diode laser at 678 nm for a light dose of 10 J/cm^2, cells were incubated for another 24 h. Cell

viability was then measured as described above using CCK-8 assay or MTT assay.

Subcellular localization. The B16-F10 cells were cultured in RPMI 1640 medium and then the cells were seeded onto thin glass-bottomed 35 mm petri dishes (NEST Biotechnology, Hangzhou, China) at 1×10^4 cells per dish and incubated for 24 h at 37℃ under 5% CO_2 atmosphere to reattach. The medium was removed and new medium containing 10 μM aspartylchlorin p_6 dimethylester (**7b**) was added, and the cells were incubated in dark for 24 h. The medium was removed and washed twice with PBS, following incubation with Mito-Tracker Green FM (200 nM, for 45 min, Molecular Probes, Life Technologies, USA), Lyso-Tracker Green DND-26 (200 nM, for 45 min, Molecular Probes, Life Technologies, USA), Golgi-Traker Green (5 μM**,** for 30 min, Molecular Probes, Yeasen, China), and ER-Traker Green (1 μM**,** for 30 min**,** Molecular Probes, Yeasen, China) at 37℃ in a 5% CO_2 incubator. Then both the medium and the trackers were removed and washed 3 times with PBS and the cells were examined using a Leica TCS SP5 spectral confocal microscope equipped with Argon-Heli-umNenon (Ar-HeNe) laser. Mito-Tracker, Lyso-Tracker, Golgi-Traker, ER-Traker and compound **7b** were respectively excited at the wavelength of 488, 488, 488, 488, 633 nm and the signals from different probes were acquired in a sequential scan mode.

Apoptosis measurement by Annexin V/PI staining. B16-F10 cells in the long-phase were seeded into six-well culture plate and incubated with compound **7b** (2.0, 5.0 μM). After 24 h, the cells were exposed to the laser at 678 nm for a light dose of 10 J/cm^2, then the cells were incubated in a 5% CO_2 incubator at 37℃ for 24 h. After that, apoptotic cells and necrotic cells were analyzed by double staining with Alexa Fluor 488 annexin V and propidium iodide (PI) (BD, USA) following the manufacturer's instructions. Cells were co-stained with 5 μL PI and immediately analyzed using Beckman Cyanflow Cytometer (Beckman,USA). The percentage of apoptotic (annexinþ/PI) and necrotic (annexinþ/PI) cells was determined using software.[55]

***In vivo* phototoxicity.** The potential PDT efficacy of aspartylchlorin p_6 dimethylester (**7b**) on B16-F10 bearing mice was investigated by irradiation with the diode laser at 678 nm. The B16-F10 bearing C57BL/6 mice

were randomly divided into 3 groups, including negative control, **7b** (1 mg/kg), and verteporfin (2 mg/kg), each group contained 5 mice. Two hours after the intravenous administration, compound 7b and verteporfin group were anesthetized and their tumor sites were irradiated with laser light (250 mW/cm^2) for 10 min, and the total light dose was 150 J/cm^2. After the treatment, the tumor was measured with a caliper, and recorded the survival of mice daily. The statistical differences between groups with respect to the mean tumor volume were evaluated by using SPSS 19.0 for windows software. The significance was accepted at $P < 0.05$.

■ ASSOCIATED CONTENT

Supporting Information

The Supporting Information is available free of charge on the ACS Publications website at DOI: XXXXXX/acs.jmedchem.XXXXXXX.

^1H and ^{13}C NMR spectra (Figure S1-S9), high resolution mass spectra (Figure S10-S17) and HPLC purity spectra (Figure S18-S23).

SMILES data (CSV)

■ AUTHOR INFORMATION

Corresponding Authors

* (H.Z.) Phone / Fax: +86 21 81870944. E-mail: zinnia69@163.com.

* (C. S.) Phone / Fax: +86 21 81871239. E-mail: shengcq@hotmail.com.

* (J.Y.) Phone / Fax: +86 21 81871243. E-mail: yaojz@sh163.net.

Author Contributions

† Zhi Meng, Bin Yu and Guiyan Han contributed equally to this work.

The manuscript was written through contributions of all authors. All authors have given approval to the final version of the manuscript.

Notes

The authors declare no competing financial interest.

■ ACKNOWLEDGMENT

This work was supported by the Natural Science Foundation of China (Grant Nos. 81172950 and 61275216), the Key Project of Science and Technology Commission of Shanghai (Grant No. 11431920400 and 11431920401) and the Project of Science and Technology Commission of Shanghai (Grant No. 11430723200 and 11430723201).

■ ABBREVIATIONS LIST

PS, photosensitizer; PDT, photodynamic therapy; BCPDs, benzochloroporphyrin derivatives; BCPD-18MA, benzochloroporphyrin p_6 dimethylester *cis*-isomer; THF, tetrahydrofuran; DDQ, 2, 3-dichloro-5, 6-dicyano-1, 4-benzoquine; DMAD, dimethyl acetylenedicarboxylate; EDCI, 1-ethyl-3-(3-dimethylaminopropyl)-carbodiimide hydrochlorate; DMF, dimethylformamide; DMSO, dimethylsulfoxide; THF, tetrahydrofuran; DBU, 1,8-diazabicyclo[5.4.0]undec-7-ene; TFA, trifluoroactic acid; DIPEA, N,N-diisopropylethylamine; HOBt, 1-hydroxybenzotriazole; HPLC, high performance liquid chromatography; PBS, phosphate buffered saline; PI, propidium iodide; FBS, fetal bovine serum; EPR, enhanced permeability and retention.

■ REFERENCES

(1) Agostinis, P.; Berg, K.; Cengel, K. A.; Foster, T. H.; Girotti, A. W.; Gollnick, S. O.; Hahn, S. M.; Hamblin, M. R.; Juzeniene, A.; Kessel, D. Photodynamic therapy of cancer: an update. *Ca-Cancer J. Clin.* **2011,** *61*, 250-281.

(2) Kousis, P. C.; Henderson, B. W.; Maier, P. G.; Gollnick, S. O. Photodynamic therapy enhancement of antitumor immunity is regulated by neutrophils. *Cancer Res.* **2007,** *67*, 10501-10510.

(3) Tomé, J. P.; Neves, M. G.; Tomé, A. C.; Cavaleiro, J. A.; Soncin, M.; Magaraggia, M.; Ferro, S.; Jori, G. Synthesis and antibacterial activity of new poly-S-lysine-porphyrin conjugates. *J. Med. Chem.* **2004,** *47*, 6649-6652.

(4) Zou, Q.; Zhao, H.; Zhao, Y.; Fang, Y.; Chen, D.; Ren, J.; Wang, X.; Wang, Y.; Gu, Y.; Wu, F. Effective two-photon excited photodynamic therapy of xenograft tumors sensitized bywater-soluble bis (arylidene) cycloalkanone photosensitizers. *J. Med. Chem.* **2015,** *58*, 7949-7958.

(5) Vakrat-Haglili, Y.; Weiner, L.; Brumfeld, V.; Brandis, A.; Salomon, Y.; Mcllroy, B.; Wilson, B. C.; Pawlak, A.; Rozanowska, M.; Sarna, T. The microenvironment effect on the generation of reactive oxygen species by Pd-bacteriopheophorbide. *J. Am. Chem. Soc.* **2005,** *127*, 6487-6497.

(6) Dąbrowski, J. M.; Arnaut, L. G. Photodynamic therapy (PDT) of cancer: From local to systemic treatment. *Photochem. Photobio. Sci.* **2015,** *14*, 1765-1780.

(7) Mroz, P.; Huang, Y.-Y.; Szokalska, A.; Zhiyentayev, T.; Janjua, S.; Nifli, A.-P.; Sherwood, M. E.; Ruzié, C.; Borbas, K. E.; Fan, D. Stable synthetic bacteriochlorins overcome the resistance of melanoma to photodynamic therapy. *FASEB J.* **2010,** *24*, 3160-3170.

(8) Lovell, J. F.; Liu, T. W.; Chen, J.; Zheng, G. Activatable photosensitizers for imaging and therapy. *Chem. Rev.* **2010,** *110*, 2839-2857.

(9) Celli, J. P.; Spring, B. Q.; Rizvi, I.; Evans, C. L.; Samkoe, K. S.; Verma, S.; Pogue, B. W.; Hasan, T. Imaging and photodynamic therapy: mechanisms, monitoring, and optimization. *Chem. Rev.* **2010,** *110*, 2795-2838.

(10) Yano, S.; Hirohara, S.; Obata, M.; Hagiya, Y.; Ogura, S.-i.; Ikeda, A.; Kataoka, H.; Tanaka, M.; Joh, T. Current states and future views in photodynamic therapy. *J. Photochem. Photobiol., C* **2011,** *12*, 46-67.

(11) Dąbrowski, J. M.; Arnaut, L. G.; Pereira, M. M.; Urbańska, K.; Simões, S.; Stochel, G.; Cortes, L. Combined effects of singlet oxygen and hydroxyl radical in photodynamic therapy with photostable bacteriochlorins: evidence from intracellular fluorescence and increased photodynamic efficacy in *vitro*. *Free Radical Biol. Med.* **2012,** *52*, 1188-1200.

(12) Krzykawska-Serda, M.; Dąbrowski, J. M.; Arnaut, L. G.; Szczygieł, M.; Urbańska, K.; Stochel, G.; Elas, M.

The role of strong hypoxia in tumors after treatment in the outcome of bacteriochlorin-based photodynamic therapy. *Free Radical Biol. Med.* **2014,** *73*, 239-251.

(13) Cloonan, S. M.; Elmes, R.-B. M.; Erby, M.; Bright, S. A.; Poynton, F. E.; Nolan, D. E.; Quinn, S. J.; Gunnlaugsson, T.; Williams, D. C. Detailed biological profiling of a photoactived and apoptosis inducing pdppz ruthenium (II) polypyridyl complex in cancer cells. *J. Med. Chem*. **2015**, *58*, 4494-4505.

(14) Drogat, N.; Gady, C.; Granet, R.; Sol, V. Design and synthesis of water-soluble polyaminated chlorins and bacteriochlorins–with near-infrared absorption. *Dyes Pigm.* **2013,** *98*, 609-614.

(15) Allison, R. R.; Downie, G. H.; Cuenca, R.; Hu, X.-H.; Childs, C. J.; Sibata, C. H. Photosensitizers in clinical PDT. *Photodiagn. Photodyn. Ther.* **2004,** *1*, 27-42.

(16) Kessel, D. Determinants of photosensitization by mono-L-aspartylchlorin e6. *Photochem. Photobiol.* **1989**, *49*, 447–452.

(17) Bakri, S. J.; Kaiser, P. K. Verteporfin ocular photodynamic therapy. *Expert Opin. Pharmacother.* **2004,** *5*, 195-203.

(18) Huggett, M.; Jermyn, M.; Gillams, A.; Illing, R.; Mosse, S.; Novelli, M.; Kent, E.; Bown, S.; Hasan, T.; Pogue, B. Phase I/II study of verteporfin photodynamic therapy in locally advanced pancreatic cancer. *Br. J. Cancer* **2014,** *110*, 1698-1704.

(19) Pereira, M. M.; Monteiro, C. J.; Simoes, A. V.; Pinto, S. M.; Abreu, A. R.; Sá, G. F.; Silva, E. F.; Rocha, L. B.; Dąbrowski, J. M.; Formosinho, S. J. Synthesis and photophysical characterization of a library of photostable halogenated bacteriochlorins: an access to near infrared chemistry. *Tetrahedron* **2010,** *66*, 9545-9551.

(20) Borbas, K. E.; Lindsey, J. S. Swallowtail bacteriochlorins. lipophilic absorbers for the near-infrared. *Org. Lett.* **2008,** *10*, 1931-1934.

(21) Huang, Y.-Y.; Mroz, P.; Zhiyentayev, T.; Sharma, S. K.; Balasubramanian, T.; Ruzié, C.; Krayer, M.; Fan, D.; Borbas, K. E.; Yang, E. *In vitro* photodynamic therapy and quantitative structure-activity relationship studies

with stable synthetic near-infrared-absorbing bacteriochlorin photosensitizers. *J. Med. Chem.* **2010,** *53*, 4018-4027.

(22) Huang, Y. Y.; Balasubramanian, T.; Yang, E.; Luo, D.; Diers, J. R.; Bocian, D. F.; Lindsey, J. S.; Holten, D.; Hamblin, M. R. Stable synthetic bacteriochlorins for photodynamic therapy: role of dicyano peripheral groups, central metal substitution (2H, Zn, Pd), and Cremophor EL delivery. *ChemMedChem* **2012,** *7*, 2155-2167.

(23) Saavedra, R.; Rocha, L. B.; Dąbrowski, J. M.; Arnaut, L. G. Modulation of biodistribution, pharmacokinetics, and photosensitivity with the delivery vehicle of a bacteriochlorin photosensitizer for photodynamic therapy. *ChemMedChem* **2014,** *9*, 390-398.

(24) Rocha, L. B.; Gomes-da-Silva, L. C.; Dąbrowski, J. M.; Arnaut, L. G. Elimination of primary tumours and control of metastasis with rationally designed bacteriochlorin photodynamic therapy regimens. *Eur. J. Cancer* **2015,** *51*, 1822-1830.

(25) Arnaut, L. G.; Pereira, M. M.; Dabrowski, J. M.; Silva, E. F.; Schaberle, F. A.; Abreu, A. R.; Rocha, L. B; Barsan, M. M.; Urbanska, K.; Stochel, G,; Brett, C. A. Photodynamic therapy efficacy enhanced by dynamics: the role of charge transfer and photostability in the selection of photosensitizers. *Chem. Eur. J.* **2014**, *20*, 5346-5357.

(26) Yao, J.; Zhang, W.; Sheng, C.; Miao, Z.; Yang, F.; Yu, J.; Zhang, L.; Song, Y.; Zhou, T.; Zhou, Y. Design, synthesis, and *in vitro* photodynamic activities of benzochloroporphyrin derivatives as tumor photosensitizers. *Bioorg. Med. Chem. Lett.* **2008**, *18*, 293-297.

(27) Zhang, J.; Deng, L.; Yao, J.; Gu, P.; Yang, F.; Wang, X.; Liu, W.; Zhang, Y.; Ke, X.; Jing, X. Synthesis and photobiological study of novel chlorin photosensitizer BCPD-18MA for photodynamic therapy. *Bioorg. Med. Chem.* **2011,** *19*, 5520–5528.

(28) Tamiaki, H.; Isoda, Y.; Tanaka, T.; Machida, S. Synthesis of chlorophyll–amino acid conjugates as models for modification of proteins with chromo/fluorophores. *Biorg. Med. Chem*. **2014**, *22*, 1421-1428.

(29) Kwitniewski, M.; Juzeniene, A.; Ma, L. W.; Glosnicka, R.; Graczyk, A.; Moan, J. Diamino acid derivatives

of PpIX as potential photosensitizers for photodynamic therapy of squamous cell carcinoma and prostate cancer: *in vitro* studies. *J. Photochem. Photobiol. B* **2009,** *94*, 214–222.

(30) Roberts, W. G.; Shiau, F. Y.; Nelson, J. S.; Smith, K. M.; Berns, M. W. In vitro characterization of monoaspartyl chlorin e6 and diaspartyl chlorin e6 for photodynamic therapy. *J. Natl. Cancer Inst.* **1988,** *80*, 330-336.

(31) Serra, V. V.; Zamarr, A.; oacute; Faustino, M. A. F.; Cruz, I. D. L.; Bl, A.; aacute; zquez; Rodrigues, J. M. M.; Neves, M. G. P. M. S.; Cavaleiro, J. A. S.; Juarranz, A.; Sanz-Rodr, F.; iacute; guez. New porphyrin amino acid conjugates: synthesis and photodynamic effect in human epithelial cells. *Bioorg. Med. Chem.* **2010,** *18*, 6170–6178.

(32) Wang, H. M.; Jiang, J. Q.; Xiao, J. H.; Gao, R. L.; Lin, F. Y.; Liu, X. Y. Porphyrin with amino acid moieties: a tumor photosensitizer. *Chem. Biol. Interact.* **2008,** *172*, 154-158.

(33) Baldea, I.; Olteanu, D. E.; Bolfa, P.; Ion, R. M.; Decea, N.; Cenariu, M.; Banciu, M.; Sesarman, A. V.; Filip, A. G. Efficiency of photodynamic therapy on WM35 melanoma with synthetic porphyrins: Role of chemical structure, intracellular targeting and antioxidant defense. *J. Photochem. Photobiol. B* **2015,** *151*, 142-152.

(34) Siddiqui, I. A.; Bharali, D. J.; Nihal, M.; Adhami, V. M.; Khan, N.; Chamcheu, J. C.; Khan, M. I.; Shabana, S.; Mousa, S. A.; Mukhtar, H. Excellent anti-proliferative and pro-apoptotic effects of (−)-epigallocatechin-3-gallate encapsulated in chitosan nanoparticles on human melanoma cell growth both *in vitro* and *in vivo*. *Nanomed.- Nanotech.* **2014,** *10*, 1619-1626.

(35) Rapozzi, V.; Zorzet, S.; Zacchigna, M.; Drioli, S.; Xodo, L. E. The PDT activity of free and pegylated pheophorbide a against an amelanotic melanoma transplanted in C57/BL6 mice. *Invest. New Drugs* **2013,** *31*, 192-199.

(36) Yao, J. Z.; Xu, D. Y.; Chen, W. H.; Liu, J. F.; Dong, J. C. Degradation of silkworm excrement crude chlorophyll and synthesis of chlorin p_6 amide derivatives. *Chin. J. Pharm.* **1999**, *30*, 403-406 (in Chinese).

(37) Yao, J. Z.; Liu, J. F.; Zhang, W. N.; Zhou, Y. J.; Zhu, J.; LU, J. G.; Wang, X. Y.; Li, K. Synthesis of chlorin p_6 ether derivatives. *Chin. J. Org. Chem.* **2001**, *21*, 458-462 (in Chinese).

(38) Young R. H.; Brewer D.; Keller R. A. Determination of rate constants of reaction and lifetimes of singlet oxygen in solution by a flash photolysis technique. *J. Am. Chem. Soc.* **1973**, *95*, 375-379.

(39) Jiang, Z.; Liu, N.; Dong, G.; Jiang, Y.; Liu, Y.; He, X.; Huang, Y.; He, S.; Chen, W.; Li, Z.; Yao, J.; Miao, Z.; Zhang, W.; Sheng, C. Scaffold hopping of sampangine: discovery of potent antifungal lead compound against aspergillus fumigatus and cryptococcus neoformans. *Bioorg. Med. Chem. Lett.* **2014,** *24*, 4090-4094.

(40) Gryshuk, A. L.; Yihui, C.; William, P.; Tymish, O.; Allan, O.; Pandey, R. K. *In vivo* stability and photodynamic efficacy of fluorinated bacteriopurpurinimides derived from bacteriochlorophyll-a. *J. Med. Chem.* **2006,** *49*, 1874-1881.

(41) Chen, Y.; Graham, A.; Potter, W.; Morgan, J.; Vaughan, L.; Bellnier, D. A.; Henderson, B. W.; Oseroff, A.; Dougherty, T. J.; Pandey, R. K. Bacteriopurpurinimides: highly stable and potent photosensitizers for photodynamic therapy. *J. Med. Chem.* **2002,** *45*, 255-258.

(42) Chen, Y.; Zheng, X.; Dobhal, M. P.; Gryshuk, A.; Morgan, J.; Dougherty, T. J.; Oseroff, A.; Pandey, R. K. Methyl pyropheophorbide-a analogues: potential fluorescent probes for the peripheral-type benzodiazepine receptor. Effect of central metal in photosensitizing efficacy. *J. Med. Chem.* **2005**, *48*, 3692-3695.

(43) Chen, Y.; Sajjad, M.; Wang, Y.; Batt, C.; Nabi, H. A.; Pandey, R. K. TSPO 18 kDa (PBR) targeted photosensitizers for cancer imaging (PET) and PDT. *ACS Med. Chem. Lett.* **2010,** *2*, 136-141.

(44) Yu, Z.; Sun, Q.; Pan, W.; Li, N.; Tang, B. A near-infrared triggered nanophotosensitizer inducing domino effect on mitochondrial reactive oxygen species burst for cancer therapy. *ACS nano* **2015**, *9*, 11064-11074.

(45) Hariharan, N.; Zhai, P.; Sadoshima, J. Oxidative stress stimulates autophagic flux during ischemia/reperfusion. *Antioxid. Redox signaling* **2011**, *14*, 2179-2190.

(46) Zheng, Y.; Yin, G.; Le, V.; Zhang, A.; Chen, S.; Liang, X.; Liu, J. Photodynamic-therapy activates immune

response by disrupting immunity homeostasis of tumor cells, which generates vaccine for cancer therapy. *Int. J. Biol. Sci*. **2016**, *12*, 120-132.

(47) Jinadasa, R. G. W.; Xiaoke, H.; Vicente, M. G. A. H.; Smith, K. M. Syntheses and cellular investigations of 17(3)-, 15(2)-, and 13(1)-amino acid derivatives of chlorin e(6). *J. Med. Chem.* **2011,** *54*, 7464-7476.

(48) Rangasamy, S.; Ju, H.; Um, S.; Oh, D.-C.; Song, J. M. Mitochondria and DNA targeting of 5, 10, 15, 20-tetrakis (7-sulfonatobenzo [b] thiophene) porphyrin-induced photodynamic therapy via intrinsic and extrinsic apoptotic cell death. *J. Med. Chem*. **2015**, *58*, 6864-6874.

(49) Furre, I. E.; Moller, M. T.; Shahzidi, S.; Nesland, J. M.; Peng, Q. Involvement of both caspase-dependent and -independent pathways in apoptotic induction by hexaminolevulinate-mediated photodynamic therapy in human lymphoma cells. *Apoptosis* **2006**, *11*, 2031-2042.

(50) Wawrzynska, M.; Kałas, W.; Biały, D.; Zioło, E.; Arkowski, J.; Mazurek, W.; Strzadała, L. *In vitro* photodynamic therapy with chlorin e6 leads to apoptosis of human vascular smooth muscle cells. *Arch. Immunol. Ther. Exp*. **2010**, *1*, 67-75.

(51) Chiou, J. F.; Wang, Y. H.; Jou, M. J.; Liu, T. Z.; Shiau, C. Y. Verteporfin-photoinduced appoptosis in HepG2 cells mediated by reactive oxygen and nitrogen species intermediates. *Free Radical Res*. **2010**, *2*, 155-170.

(52) Gabizon, A.; Shmeeda, H.; Barenholz, Y. Pharmacokinetics of pegylated liposomal doxorubicin: review of animal and human studies. *Clin. Pharmacokinet.* **2003**, *42*, 419-36.

(53) Lin H.; Shen Y.; Chen D.; Lin L.; Wilson B. C.; Li B.; Xie S. Feasibility study on quantitative measurements of singlet oxygen generation using singlet oxygen sensor green. *J. Fluoresc*. **2013**, *23*, 41-47.

(54) Li, H.; Huang, W.; Luo, R.The microRNA-325 inhibits hepatocellular carcinoma progression by targeting high mobility group box 1. *Diagn. Pathol.* **2015**, *10*, 117-128.

(55) Wang, Y.; Yang, F.; Zhang, H. X.; Zi, X. Y.; Pan, X. H.; Chen, F.; Luo, W. D.; Li, J. X.; Zhu, H. Y.; Hu, Y. P. Cuprous oxide nanoparticles inhibit the growth and metastasis of melanoma by targeting mitochondria. *Cell Death*

Dis. **2013,** *4*, 3133-3145.

Table of Contents Graphic

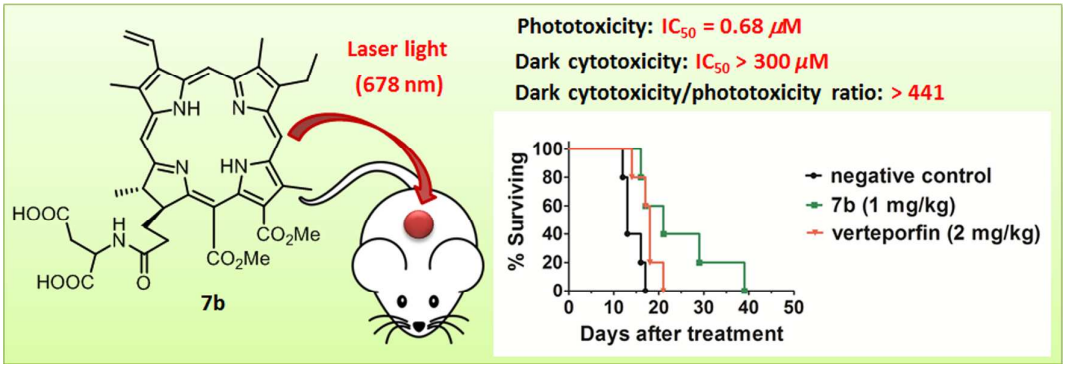

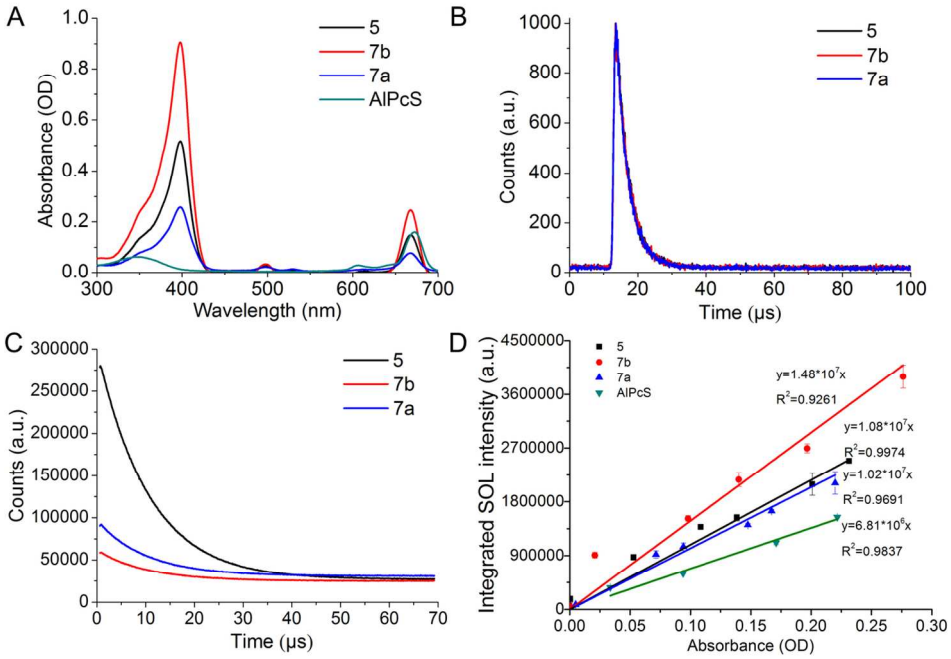

Figure 1. Photophysical properties of the target compounds. (A) UV absorption spectra of 5, 7a, 7b and AlPcS in methanol; (B) The time-resolved fluorescence of 5, 7a, 7b; (C) 1O2 luminescence spectra (λex = 532 nm) of 5, 7a, 7b; (D) Plot of 1O2 luminescence counts against the absorbance for 5, 7a, 7b and AlPcS in methanol. The error bars represent the standard deviation of the mean of three independent measurements.
128x88mm (300 x 300 DPI)

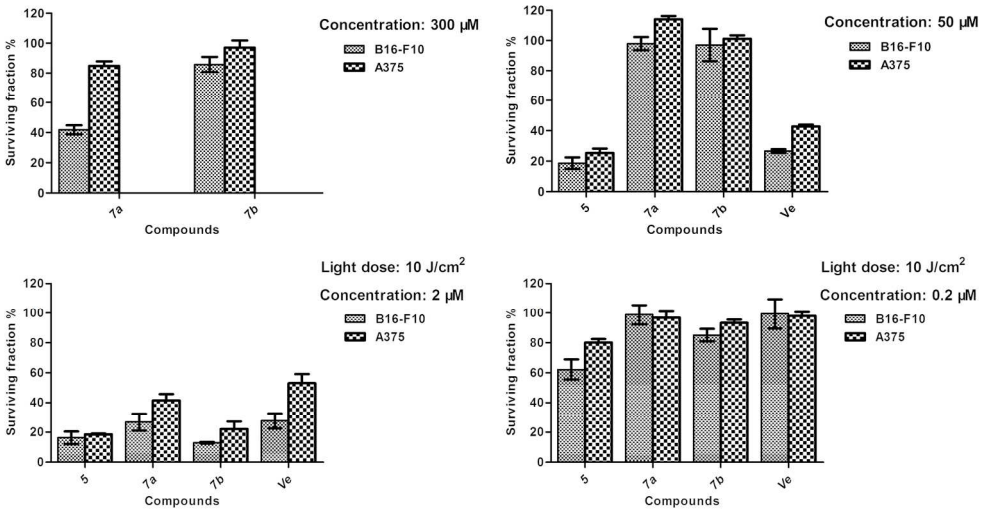

Figure 2. Survival fraction of B16-F10 and A375 cells treated by 5, 7a,7b and verteporfin ("ve") at the concentrations of 300 μM and 50 μM under dark or at the concentrations of 2 μM and 0.2 μM with a light dose of 10 J/cm2 using the CCK-8 assay.
199x106mm (300 x 300 DPI)

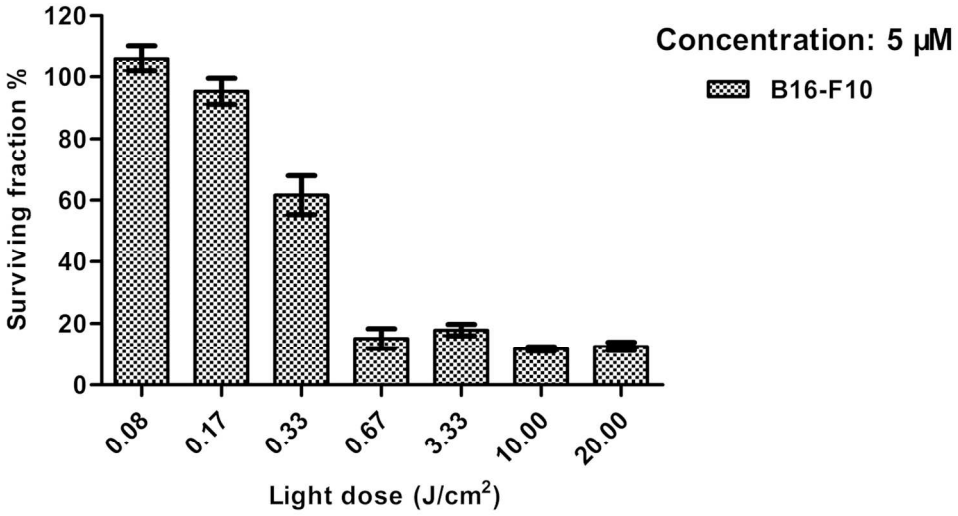

Figure 3. Survival fraction of B16-F10 cells treated by 7b with various light dosages at the concentration of 5 μM using the CCK-8 assay.
137x78mm (300 x 300 DPI)

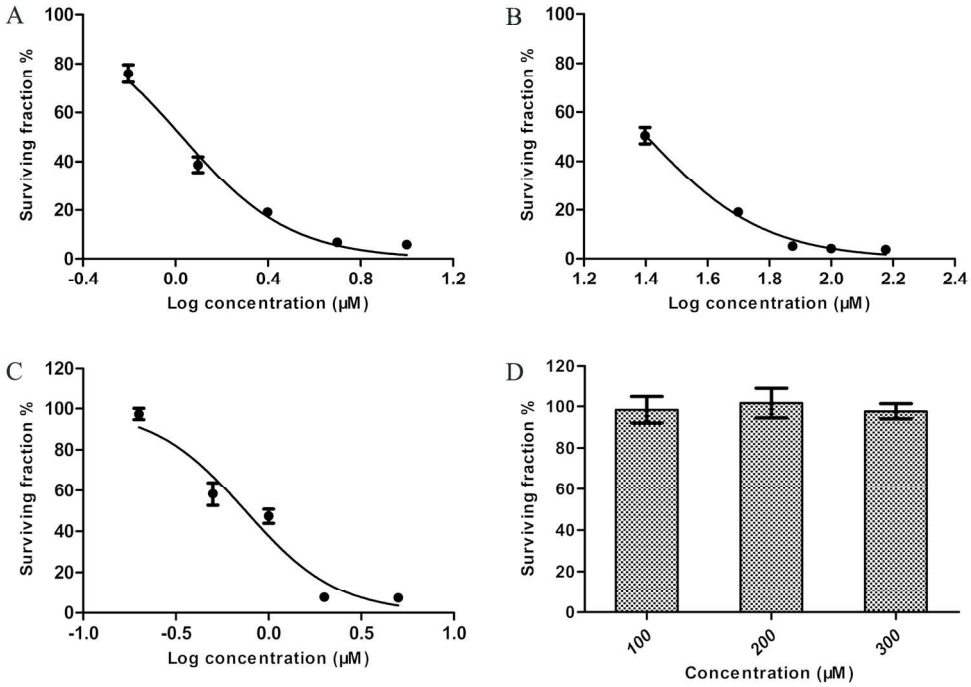

Figure 4. In vitro phototoxicity of verteporfin (A), 7b (C) and dark-toxicty of verteporfin (B), 7b (D) toward B16-F10 cells using the MTT assay.
194x140mm (300 x 300 DPI)

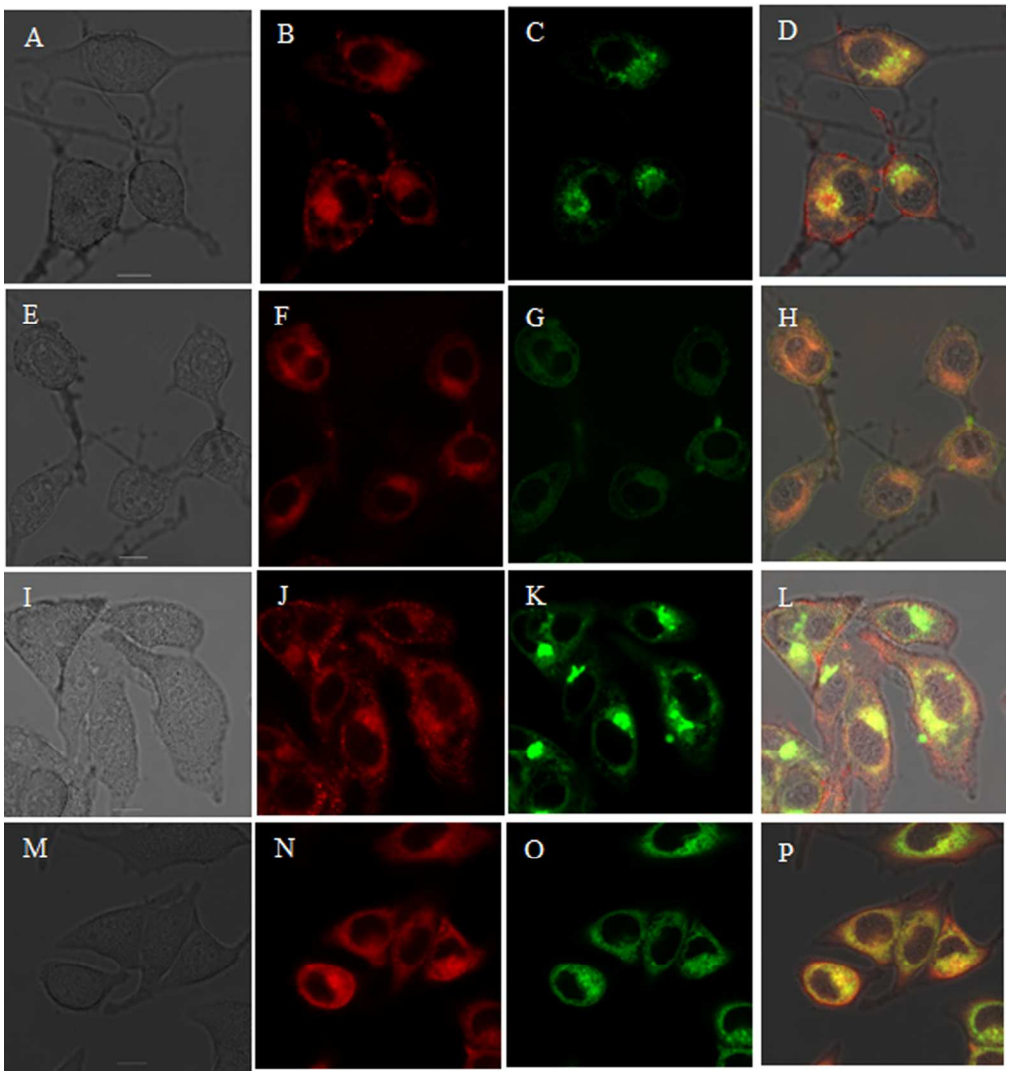

Figure 5. Subcellular location of 7b in B16-F10 cells at 10 μM for 24 h: (A, E, I, M) phase contrast; (B, F, J, N) red fluorescence corresponds to 7b; (C) Mito Tracker Green fluorescence; (G) Lyso Tracker Green fluorescence; (K) Golgi Tracker Green fluorescence; (O) ER Tracker Green fluorescence; (D, H, L, P) overlays of organelle trackers with 7b fluorescence. Scale bar: 10 um.
152x163mm (300 x 300 DPI)

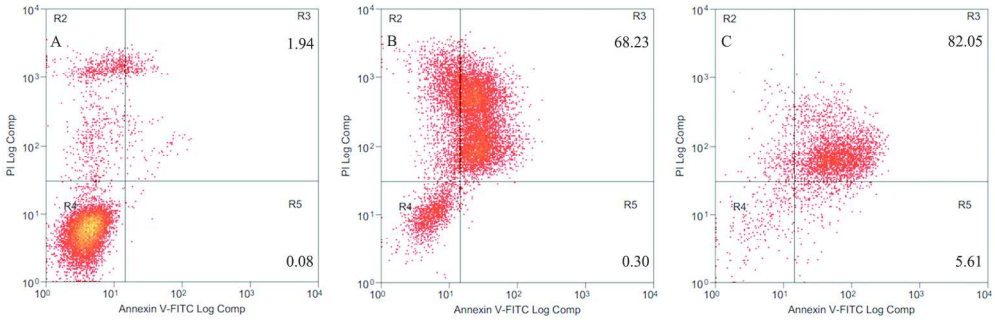

Figure 6. Flow cytometry analysis of B16-F10 cells with Annexin V/PI double staining after PDT: (A) Blank; (B) Treated with 2.0 μM of 7b at a light dose of 10 J/cm2; (C) Treated with 5.0 μM of 7b at a light dose of 10 J/cm2. UL (upper left quadrant), Annexin V (-) PI (+), cell fragment; UR (upper right quadrant), Annexin V (+) PI (+), necrosis or the late period apoptosis; LL (lower left quadrant), Annexin V (-) PI (-), survival cell; LR (lower right quadrant), Annexin V (+) PI (-), early period apoptosis.
224x73mm (300 x 300 DPI)

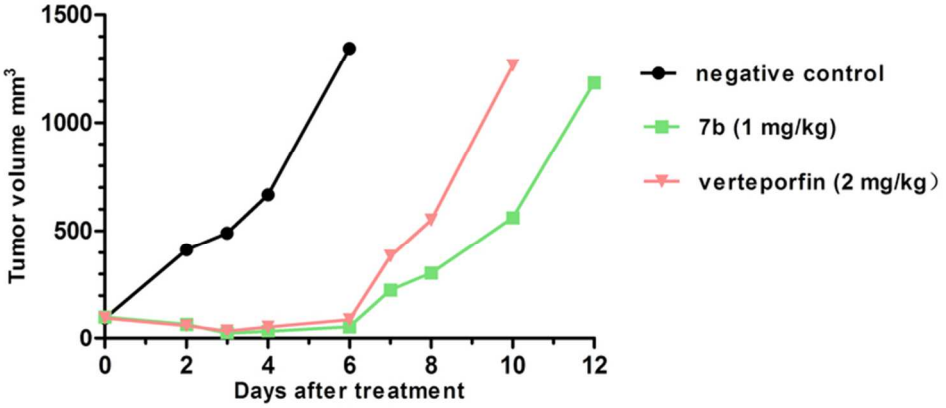

Figure 7. PDT efficacy on C57BL/6 mice bearing B16-F10 tumor. The mice were divided into 3 groups (5 mice in each group): negative control (black line), 7b-PDT (1 mg/kg, green line), verteporfin-PDT (2 mg/kg, red line). The tumors were irradiated with laser light (678 nm, 150 J/cm2) at 2 h after intravenous administration.
71x32mm (300 x 300 DPI)

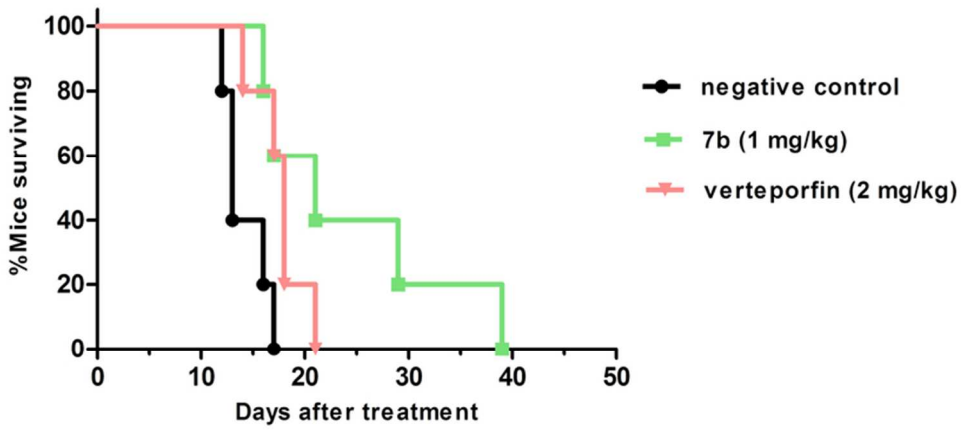

Figure 8. Kaplan-Meier survival curve of C57BL/6 mice bearing B16-F10 tumor. P < 0.05 for verteporfin-PDT group and 7b-PDT group, compared with negative control by log-rank test (n = 5).
72x35mm (300 x 300 DPI)

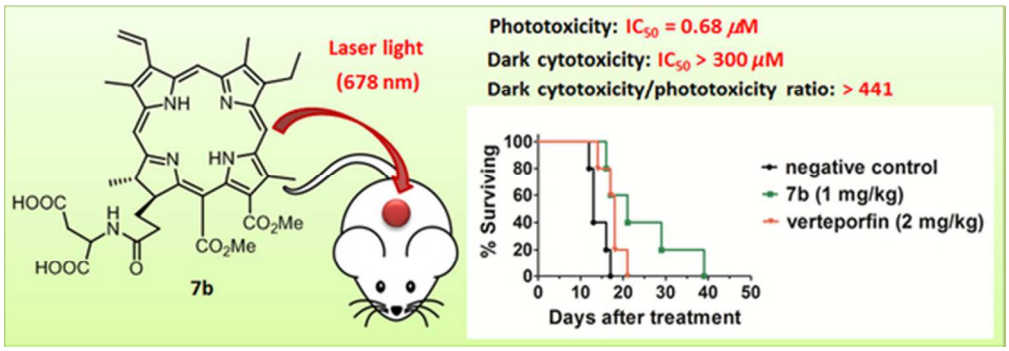

Table of Contents Graphic
50x17mm (300 x 300 DPI)